The Potential of Alkali-Treated Sisal Fiber/Granite Reinforced Hybrid Composites for Automotive Semi-Trailer Loading Floor Applications

A Thesis submitted in partial fulfillment of the requirements for the degree of

MSc.

in

Product Design and Development

By

Semere Ayahuney

Under the supervision of

Abrha Gebregergs (Assistant Professor)

Mekelle University

Ethiopia Institute of Technology - Mekelle (EiT-M)

School of Mechanical and Industrial Engineering (SMIE)

June 2025

Mekelle, Ethiopia

ACKNOWLEDGEMENTS

This study would not have been possible without the valuable contributions of many individuals and organizations. First and foremost, I am deeply grateful to my supervisor, Dr. Abrha Gebregergs, for his exceptional professional support, continuous encouragement, and invaluable guidance throughout the entire process. I would also like to extend my sincere thanks to my friends for their support and dedicated work in the laboratory at EIT-M. Their remarkable assistance in collecting materials, preparing the composite laminates, and cutting the test samples was crucial to the success of this work. My appreciation goes to the School of Mechanical and Industrial Engineering and the School of Civil Engineering at the Ethiopian Institute of Technology Mekelle (EIT-M), Mekelle University, for providing materials, laboratory services, and research funding. Without their support, this work would not have reached its current form. Last but not least, my heartfelt thanks go to my family and friends for their unwavering support and encouragement throughout the past few years, which greatly contributed to the completion of this dissertation.

ABSTRACT

Natural fiber reinforced composites offer a sustainable alternative in the composite industry due to their low density, high specific strength, and eco-friendliness. Sisal fibers, abundantly grown in northern Ethiopia, are attractive for their low cost and favorable mechanical properties but are limited by their inherent weaknesses in mechanical strength, water absorption resistance, and durability. This research focuses on enhancing these properties in sisal/polyester composites for automotive applications, specifically for a semi-trailer loading floor. The study investigates the efficacy of alkali (NaOH) treatment of sisal fibers and hybridization with granite powder as a filler to improve mechanical performance and water resistance. Experimental evaluations determined that a composite with 30 wt.% alkali-treated sisal fibers and 5 wt.% granite powder (E8) exhibited the best overall mechanical properties (tensile, flexural, compressive, and impact strengths) and significantly reduced water absorption. The Technique for Order Preference by Similarity to Ideal Solution (TOPSIS) was employed to select this optimal composite formulation from various alternatives. Subsequently, a Genetic Algorithm (GA) was used to optimize the design of a sisal/granite hybrid composite loading floor, achieving an approximate weight reduction of 64.3% compared to a conventional steel counterpart. Finite Element Analysis (FEA) validated the optimized design, confirming a peak stress of 43.9 MPa and a minimum factor of safety of 2.19 in the most critical ply, meeting the design constraints. The maximum deflection was 1.459 mm, well within serviceable limits. The findings demonstrate the potential of alkali-treated sisal/granite polyester composites as a lightweight, durable, and sustainable material for semi-structural transport applications.

KEYWORDS

Alkali treatment

Polyester

Hybrid composite

Sisal fiber

Granite powder

Agglomeration

TOPSIS (Technique for order preference by similarity to ideal solution)

GA (Genetic Algorithm)

FEA (Finite Element Analysis)

Weight reduction

Tensile strength

Compressive strength

Water absorption

Density

Flexural strength

Impact strength

DECLARATION

Candidate's Declaration

I affirm that this thesis is based on my independent research, except where I have clearly stated otherwise. I have adhered to all the principles of academic honesty and integrity, ensuring that I have not misinterpreted, fabricated, or falsified any information, data, facts, or sources in my work. I understand that violating these principles can lead to disciplinary actions by the Institute and other parties if I have not properly credited them or obtained the necessary permissions.

Name of candidate: **Semere Ayahuney** Signature: _____Date: _____

Advisor's Declaration

This is to certify that the above declaration made by the candidate is correct to the best of my knowledge and the thesis is adequate for the award of the degree of Master of Engineering in Automotive Engineering.

Name of Advisor: Abrha Gebregergs (PhD) Signature: _____Date_____

THESIS ACCEPTANCE APPROVAL FORM

"This is to certify that the thesis prepared by **Mr. Semere Ayahuney Tesfatsion**, entitled '***The Potential of Alkali-Treated Sisal Fiber/Granite Reinforced Hybrid Composites for Automotive Semi-Trailer Loading Floor Applications,***' has been accepted for the award of the Degree of Master of Science in Mechanical Engineering (Product Design and Development), in partial fulfillment of the requirements for the Master of Science in Mechanical Engineering at Mekelle University."

Members of the Examination Board

Dr. Kalayu Mekonen		13/06/2025
External Examiner	Signature	Date
Dr Alula Gebresas		13/06/2025
Internal Examiner	Signature	Date
Dr Abrha Gebregergs		13/06/2025
Supervisor	Signature	Date
Mr Tadesse Gebray		13/06/25
Chairman	Signature	Date

Confirmation: SMD Chair

ታደሰ ገብረ-ይ ተስፋ-ይ (MS c)
የሶሊድ መካኒክስና ዲዛይን ቼይር ሐላፊ
Tadesse Gebray Tesfay (MS.c)
Head of Solid Mechanics & Design Chair

Chair Head

Signature

13/06/2025
Date

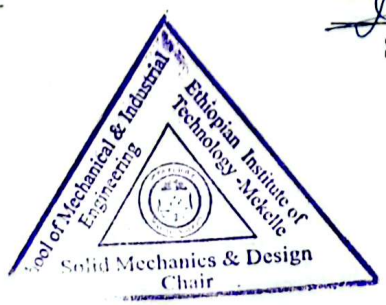

CONTENTS

LIST OF TABLES

LIST OF FIGURES

CHAPTER ONE

1 INTRODUCTION

1.1 Background

Natural fiber reinforced composites are increasingly recognized as a viable alternative to conventional materials in various industries, particularly automotive, due to their low density, commendable specific strength, and environmental benefits. Sisal fibers, abundantly available in regions like northern Ethiopia, present a promising reinforcement option owing to their low cost and inherent mechanical attributes such as good specific tensile strength and stiffness. However, the broader adoption of sisal fibers in demanding applications has been constrained by their relatively poor mechanical properties, susceptibility to water absorption, and degradation over time, which can compromise the long-term performance of sisal/polyester composites. This necessitates research focused on enhancing these characteristics. Methods such as alkali treatment have been shown to improve fiber-matrix adhesion and, consequently, the mechanical and water resistance properties of composites. Furthermore, the incorporation of filler materials, like granite powder, offers a pathway to further augment the composite's performance, contributing to increased stiffness, wear resistance, and dimensional stability. Granite, a readily available industrial byproduct, can also improve the eco-profile of the composite. This research explores the synergistic effects of alkali treatment on sisal fibers and the hybridization with granite powder within a polyester matrix. The study aims to develop an optimized sisal/granite/polyester composite tailored for automotive components, such as semi-trailer loading floors, thereby addressing the industry's demand for lightweight, sustainable, and high-performance materials.

1.2 Problem Statement

Sisal plants are abundantly available in northern Ethiopia, offering a readily accessible and drought-resistant lignocellulosic fiber source. Despite their prevalence and ease of cultivation, sisal fibers have predominantly been confined to low-value applications such as ropes, bags, and traditional crafts due to their inherent limitations, including relatively poor mechanical properties, high moisture absorption, and insufficient interfacial adhesion with polymeric matrices when used in composites. This underutilization signifies a missed opportunity for value addition and economic benefit for local communities. The automotive industry is actively seeking lightweight, sustainable, and cost-effective alternatives to traditional materials like steel to enhance fuel efficiency and reduce emissions. While natural fiber composites are promising candidates, untreated sisal fibers often fail to meet the demanding performance criteria for structural or semi-structural automotive components. Enhancing the mechanical strength, durability, and reducing the water uptake of sisal fiber-reinforced polyester composites is therefore crucial for their viable application in this sector. This research specifically addresses the challenge of improving sisal/polyester composites by employing alkali (NaOH) treatment to modify the sisal fiber surface, aiming to improve its compatibility and interfacial bonding with the polyester matrix, thereby enhancing mechanical performance. Additionally, it incorporates granite powder, an industrial byproduct, as a filler material to further enhance the composite's properties such as stiffness, wear resistance, and thermal stability, while also contributing to a more sustainable material lifecycle. A critical aspect is the systematic optimization of this hybrid composite system—determining the optimal balance of alkali-treated sisal fibers and granite powder within the polyester matrix to achieve superior performance characteristics tailored for specific automotive applications, such as semi-trailer loading floors. This involves a methodical approach to material formulation and selection, which is often lacking for this specific combination of materials. Therefore, this research confronts the problem of transforming underutilized local sisal fibers and industrial granite waste into a high-performance, lightweight, and sustainable composite material suitable for automotive applications. It aims to overcome the current limitations of sisal fibers through chemical treatment and hybridization, and to establish an optimized material system using multi-criteria decision-making techniques, thereby fostering local economic development and contributing to environmentally conscious material solutions.

1.3 Objective

1.3.1 General Objective

The general objective of this dissertation is to enhance the mechanical properties and water absorption resistance of sisal/polyester composite materials for automotive applications through the application of alkali (NaOH) treatment, granite filler hybridization, and optimization using the Technique for Order Preference by Similarity to Ideal Solution (TOPSIS) and genetic algorithm (GA).

1.3.2 Specific Objectives

- To experimentally analyze the influence of incorporating varying weight percentages (2.5%, 5%, 7.5%, 10%) of granite powder as a filler on the mechanical properties (tensile, flexural, compressive, impact), water absorption characteristics, and density of the alkali-treated sisal/polyester composites with different fiber-to-matrix ratios (20/80 and 30/70).
- To utilize the Technique for Order of Preference by Similarity to Ideal Solution (TOPSIS) method to evaluate and select the most suitable sisal/granite/polyester composite formulation for a semi-trailer loading floor application, based on a multi-criteria assessment including mechanical strength, water absorption, and density.
- To design and optimize a lightweight sisal/granite hybrid composite semi-trailer loading floor using a Genetic Algorithm (GA), with the objective of minimizing weight while satisfying structural performance constraints (e.g., Tsai-Wu failure criterion, stress and strain limits) under defined loading conditions.
- To validate the structural performance (stress distribution, deflection, and factor of safety) of the GA-optimized sisal/granite composite loading floor design using Finite Element Analysis (FEA) in Abaqus and compare its weight and potential fuel savings against a conventional steel counterpart.

1.4 Scope

This dissertation investigates the development and optimization of sisal fiber-reinforced polyester composites hybridized with granite powder for use in automotive applications, particularly semi-trailer loading floors. The study encompasses the enhancement of mechanical properties through alkali (NaOH) treatment of sisal fibers and the inclusion of granite powder as a secondary filler to improve strength, stiffness, and water resistance. The mechanical performance of the composites is comprehensively assessed through tensile, compressive, flexural, and impact testing. In addition to evaluating mechanical behavior, the study examines water absorption and density to determine the material's suitability for semi-structural components that require both durability and light weight. To identify the most effective composite formulation, a multi-criteria decision-making method—Technique for Order Preference by Similarity to Ideal Solution (TOPSIS)—is employed. The selected optimal material is then used in the structural design of a semi-trailer loading floor, with weight reduction being pursued through optimization using a Genetic Algorithm (GA). The structural performance of the GA-optimized composite floor is further validated through Finite Element Analysis (FEA) under static loading conditions, ensuring the design meets required mechanical and safety standards. Overall, the scope of this work spans materials development, experimental validation, computational optimization, and structural simulation, offering a complete framework for assessing the viability of natural fiber hybrid composites in automotive design.

1.5 Limitations

Despite its comprehensive approach, this study has certain limitations that should be acknowledged. The research is limited to evaluating the structural performance of the composite material under static loading conditions; it does not address fatigue behavior or cyclic loading, which are critical for predicting the long-term durability of automotive components. Environmental factors such as prolonged UV exposure, temperature fluctuations, and biodegradation were not studied, leaving uncertainties regarding the composite's performance in real-world service environments over extended periods. Additionally, the manufacturing process was confined to hand lay-up and compression molding techniques, which may not reflect the scalability or cost-efficiency of industrial production methods. The natural variability in sisal fiber properties, such as differences in fiber strength and diameter from batch to batch, was not thoroughly quantified or incorporated into the performance assessment, potentially affecting consistency in large-scale applications. These limitations suggest areas for future research aimed at enhancing the robustness and applicability of sisal/granite hybrid composites in demanding engineering contexts.

1.6 Organization Of the Thesis

This thesis investigates the development and optimization of sisal fiber-reinforced polyester composites hybridized with granite powder for use in automotive applications, specifically semi-trailer loading floors. The study is structured into six chapters. **Chapter One** introduces the research problem, objectives, scope, and limitations. It emphasizes the need for sustainable, lightweight materials and explores the potential of underutilized local resources such as sisal fiber and granite powder. **Chapter Two** provides a comprehensive literature review on natural fiber composites, chemical treatments, hybridization with synthetic fillers, and the challenges of water absorption. The review identifies research gaps, particularly the lack of systematic studies combining alkali-treated sisal fibers with granite powder in polyester matrices. **Chapter Three** presents the materials and fabrication methods used in this study. It outlines the selection and treatment of sisal fibers, the preparation of granite-filled polyester resin, and the hand lay-up and compression molding process used to produce the composite laminates. **Chapter Four** details the experimental procedures used to evaluate the mechanical properties of the composites, including tensile, compressive, flexural, and impact strength, as well as water absorption and density. This chapter also introduces the methodology for multi-criteria decision-making using the Technique for Order Preference by Similarity to Ideal Solution (TOPSIS), and the design optimization process using a Genetic Algorithm (GA). Furthermore, it describes the use of Finite Element Analysis (FEA) to validate the optimized design. **Chapter Five** presents the experimental and optimization results. It compares the performance of different composite formulations, identifies the optimal material using TOPSIS, and evaluates the GA-optimized design. FEA simulations are used to validate the structural integrity of the optimized composite floor. **Chapter Six** concludes the thesis by summarizing the key findings and contributions. It also outlines recommendations for future research, including fatigue testing and long-term durability studies to support broader application of natural fiber composites in structural components. This thesis contributes to the advancement of sustainable composite materials by demonstrating the effective use of locally available natural fibers and industrial byproducts, offering an eco-friendly and high-performance alternative for automotive applications.

CHAPTER TWO

2 LITERATURE REVIEW

2.1 Introduction

In recent years, there has been increasing interest in developing sustainable and environmentally friendly materials for automotive applications to minimize the ecological impact of vehicle production and use. Natural fiber-reinforced composites have emerged as a viable alternative to conventional synthetic materials for various automotive components, owing to their renewability, affordability, lightweight characteristics, and potential to reduce carbon emissions. Among these applications, the use of natural fibers in structural and semi-structural automotive components has gained significant attention. This literature review aims to examine the current advancements in the research and development of natural fiber-reinforced composites, with a particular emphasis on their suitability for automotive applications. The review will explore the effects of hybrid fillers, alkali treatment, and water absorption behavior on composite performance. Furthermore, it will highlight recent progress in optimizing these composites through material enhancements and structural design improvements to meet the demanding requirements of the automotive industry.

2.2 Sisal Fibers

Sisal fibers, a natural resource abundant in the northern region of Ethiopia, have historically been limited to traditional uses such as bags, baskets, ropes, and rugs due to their poor physical and mechanical properties. Despite their underutilization in industrial applications, sisal plants are resilient to drought and easy to cultivate, presenting a valuable opportunity to generate income for local farmers and small-scale manufacturers. By conducting ongoing research to enhance the mechanical and physical properties of sisal fibers, there is potential to elevate their industrial relevance and unlock new economic opportunities in the region.

A study conducted by Asfaw [1] on sisal plants grown in northern Ethiopia revealed that the length and tensile strength of sisal fibers vary depending on the collection sites. In a separate research by Melkamu et al. [2] the mechanical and water-absorption properties of randomly oriented short sisal fiber reinforced polyester composite were examined. The sisal fibers used in

this study were sourced from Kuha, Tigay, Ethiopia. The tensile strength of the composites was found to be lower than that of pure polyester, while other mechanical properties showed improvement. Similarly, Maurya et al. [3] conducted experiments on randomly oriented short sisal fiber reinforced epoxy composite to evaluate the tensile strength, flexural strength, and impact strength of the composite material. The composites were fabricated using the hand lay-up method with varying fiber lengths (5, 10, 15, and 20 mm) and a consistent 30% weight of sisal fiber content. The results revealed that while the tensile strength did not increase with sisal reinforcement, the flexural strength showed a 25% improvement with 15 mm sisal fiber, and a significant enhancement was observed in impact properties with 20 mm long sisal fiber. The maximum mechanical properties achieved in this study were: Flexural strength of 128 MPa, tensile strength of 40 MPa, flexural modulus of 11.896 GPa, tensile modulus of 187 MPa, and impact strength of 27.6295 kJ/m2. Similarly, research by Gupta & Srivastava [4] demonstrated improvements in the mechanical, thermal, and water absorption properties of sisal fiber reinforced epoxy composite by aligning the fibers in a unidirectional arrangement. The sisal fiber exhibited mechanical properties including a tensile strength range of 363–700 MPa, young modulus of 9–38 GPa, strain of 2.0–2.5%, and a length of 900 mm [4,5].

The mechanical properties of composites are adversely affected by water absorption [6–10]. Chaudhary et al. [8] specifically documented a significant reduction of up to 46.9% in tensile strength as a consequence of water absorption. This finding underscores the critical importance of addressing water-induced degradation to maintain the structural integrity and performance of composite materials.

Researchers have dedicated efforts towards improving the inadequate mechanical and water absorption properties of sisal fiber reinforced composites for a wide range of applications. This has been achieved through the utilization of treatments and hybridization with synthetic fibers. Various chemicals have been commonly employed in this process, including amino acids, methyl methacrylate mixed with ceric ammonium nitrate, alkali, and alkali combined with clay. Furthermore, hybrids such as glass fibers, carbon fibers, and various fillers have been incorporated to enhance the properties of these composites. The combination of these treatments and hybridizations has shown significant enhancement in the overall performance and durability of sisal fiber reinforced composites, making them suitable for diverse industrial applications.

2.3 Alkali Treatments

The treatment of sisal fibers before their use as composite reinforcement enhances the adhesive characteristics of the fiber surface, leading to improved fiber-matrix interface adhesion and increased mechanical properties. Various chemicals are utilized for this treatment, including amino acids, methyl methacrylate mixed with ceric ammonium nitrate, alkali, and alkali combined with clay [11–18]. Studies have shown significant enhancements in mechanical, water absorption, and heat resistance properties by enhancing the interfacial adhesion between fibers and polymer matrix. This improvement in interfacial adhesion is crucial for enhancing the mechanical properties of natural fiber reinforced composites [12]. Up to 16.73% improvement in impact strength of alkali-treated sisal/cattail polyester commingled hybrid composites at 20% fiber weight fractions was reported by Mbeche & Omara [19]. Fiore et al. [20] introduced a novel chemical treatment method for natural fibers using an eco-friendly and cost-effective approach based on the use of commercial sodium bicarbonate (baking soda). Sisal fibers treated with a 10% sodium bicarbonate solution for an optimized time of 120 hours exhibited improved mechanical properties due to enhanced interfacial fiber-matrix adhesion. In recent years, the eco-friendly and cost-effective treatment involving the soaking of natural fibers in a sodium bicarbonate solution has gained popularity [21–28]. Moreover, research on silane treatment of sisal fibers has demonstrated a significant transformation in the surface topography, chemical structure, and thermal degradation characteristics of sisal fibers, leading to enhanced mechanical properties of the composite [29]. The application of flame retardants such as ammonium polyphosphate (APP), magnesium hydroxide (Mg(OH)2), zinc borate (Zb), and a combination of APP with Mg(OH)2 and Zb to sisal fiber/polypropylene (PP) composites has also resulted in improved flame retardancy and thermal stability of the PP composites, while maintaining their mechanical properties undamaged[30]. Furthermore, treating sisal fibers prior to their use in composites has shown decrement in their degradation due to water absorption [10,31].

2.4 Hybridization

Fillers have emerged as effective hybrid materials for enhancing the properties of fiber-reinforced composites and reducing the overall production costs [32,33]. Researchers have explored various natural and synthetic fillers, such as granite, wood dust flour, wood charcoal, carbon nanotube fillers, and graphene powders, to enhance the performance of fiber-reinforced polymeric composite materials. [34–36] In recent years, the biodegradability, cost-effectiveness, sustainability, and eco-friendliness of natural fibers have gained the attention of researchers in developing composites by incorporating hybrid nano-fillers with natural fibers as a sustainable alternative to synthetic fibers [35–43]. Ganapathy et al. [35] investigated the impact of graphene powder on banyan aerial root fibers reinforced epoxy composites. They achieved a maximum increase of 45.4% in tensile strength and 5% in flexural strength with a 4 wt.% graphene powder content in the composite. However, a further increase in graphene content led to a decrease in mechanical properties. Saiteja et al. [36] reported the highest tensile and impact strengths in a jute-reinforced hybrid polymer composite filled with a 6% volume of carbon nanotube fillers. The flexural strength increased up to the addition of 8% volume of nanotube fillers and then decreased due to the agglomeration of nanotube fillers in the composite. Cardoso et al. [44] evaluated HDPE composites with alumina and silicon carbide for lightweight body armor. Samples A80 and A70 showed the best ballistic performance with DOP values of 15.98 mm and 17.98 mm. Ceramic reinforcements reduced tensile strength and impact resistance but increased Shore D hardness in samples A40, A50, and A60. Gebremeskel et al. [45] examined the strain rate sensitivity of PP composites with nano-clay fillers for lightweight armor. Testing showed that 5wt% nano-clay improved the strain rate sensitivity index and strength compared to 2wt% and neat PP. A new method combining stress-strain data from quasi-static and high strain rates highlighted enhanced performance, with values comparable to superplastic alloys. Dias et al. [46] explored HDPE composites with 3% montmorillonite (MMT) filler for ballistic applications. The HDPE/MMT matrix showed superior compression strength, dynamic response, and ballistic limits compared to a commercial resin matrix. The addition of filler improved fiber interaction and energy absorption, making HDPE/MMT a promising lightweight solution for ballistic protection. Haro et al.[47] studied Kevlar fiber-reinforced HDPE hybrid composites with micro (chonta wood, potato flour) and nano-fillers (silica, alumina). Tests showed synthetic nano-fillers improved stiffness (43.5%) and impact resistance, with gamma alumina achieving

the highest energy absorption. Fillers reduced crystalline peak intensity but maintained structure. Hybridization enhanced stiffness, impact resistance, and ballistic performance. Dharani Kumar et al. [48] found that adding 2wt% boron carbide (B4C) to glass fiber epoxy composites improved mechanical properties and ballistic performance, with better energy absorption and lower back face signature in tests. The filler has enhanced matrix toughening and fiber-matrix bonding, while unfilled composites showed weaker performance. Matrix hardening and strong bonding enhance toughness and energy absorption, with synergistic fillers playing a key role in strengthening energy dissipation and improving GFERC performance. [45,48]

Moreover, the use of leftovers as fillers in polymer composites has become a unique area of waste reuse techniques. Approximately 200 million tons of marble waste powder or sludge is produced annually worldwide by the marble industry, and these materials have lately been investigated as fillers for PP and epoxy resin composites [49]. Granite powder, a byproduct of the marble and granite industries, contributes to air, water, and soil pollution, disrupting ecosystems and posing environmental hazards. It is produced during processes like cutting and polishing granite stones and can also be harmful to humans if inhaled [42,50,51]. Reddy et al. [42] investigated the impact of granite powder on the mechanical and water absorption properties of fiber-reinforced polyester composites. Using Cordiadichotoma fiber and polyester matrix, the study showed that adding granite powder improved the tensile, flexural, and impact strengths of the composites. Awad et al. [52] studied the reuse of marble and granite (M&G) waste in polypropylene (PP) composites to reduce costs and promote eco-friendly production. Incorporating 0–50 wt% M&G dust improved mechanical properties, thermal stability, and water resistance, offering a practical solution for waste management and low-cost product manufacturing. Pour et al. [53] studied the use of GFRP rebars and PP fibers to enhance the shear performance of RCA concrete beams. The results showed that increasing RCA content improved the effectiveness of PP fibers, boosting ductility and deformability while reducing the risk of sudden shear failure.

2.5 Composites in Automotive Application

Advancements in the aviation and automotive industries have fostered healthy competition and spurred innovation in the modification and replacement of conventional components with advanced material-based alternatives. In the current landscape, weight reduction has become a key priority in the automotive sector, driven by the need to conserve natural resources and minimize energy consumption. This objective has been pursued through the development of high-performance materials, optimized structural design, and improved manufacturing techniques [54–57]. Optimization efforts in the automotive industry have increasingly focused on reducing the weight of structural components without compromising strength, durability, or safety. Researchers have employed techniques such as finite element analysis (FEA) and evolutionary algorithms to refine the geometry, material distribution, and configuration of components under various loading conditions. For instance, Shokrieh and Rezaei [58] demonstrated that replacing a steel automotive component with an optimized glass/epoxy composite counterpart can achieve significant reductions in stress levels and natural frequencies while achieving up to 80% weight savings. The optimized component featured geometrical variations such as a linear increase in thickness and a tapered width to ensure uniform stress distribution. Common design constraints in such optimization studies include the Tsai–Wu failure criterion and displacement limits [58–60]. More recently, Ma et al. [61] proposed an effective algorithm for structural optimization of composite automotive parts, achieving compliance with bending stiffness and stress requirements. Similarly, Wang et al. [62] developed a lightweight composite structure for a semi-trailer application using glass fiber composites, achieving a 64.3% weight reduction compared to a steel equivalent while also improving fatigue performance by over 60%. These advancements underscore the transformative potential of material and structural optimization in achieving lightweight, durable, and high-performance solutions for the next generation of automotive components.

2.6 Literature Gaps

Extensive research has explored natural and synthetic fillers—like graphene, carbon nanotubes, nano-clays, and waste powders—in various polymeric composites for applications ranging from ballistic protection to general structural components. Many studies report improvements in strength, impact resistance, and thermal behavior through such hybridizations. However, a specific gap exists in the systematic development and optimization of sisal fiber-reinforced polyester composites utilizing granite powder as functional filler, explicitly targeting automotive structural applications like semi-trailer loading floors. While granite powder, an industrial byproduct with potential environmental concerns if not managed, has shown promise for enhancing mechanical and water-resistant properties in some composite systems, its efficacy and interaction within sisal/polyester matrices remain largely underexplored. Furthermore, although alkali (NaOH) treatment is a known method for improving fiber-matrix adhesion in natural fiber composites, there is limited research that comprehensively evaluates its combined effect with granite powder fillers on the mechanical performance, water absorption characteristics, and long-term durability factors of sisal/polyester composites. Additionally, while optimization techniques such as Genetic Algorithms (GA) have been applied in composite design, the strategic use of the Technique for Order Preference by Similarity to Ideal Solution (TOPSIS) for selecting optimal material formulations specifically within the context of sisal/granite/polyester composites for such applications is underutilized. Therefore, this research addresses these critical gaps by systematically investigating the combined effects of alkali-treated sisal fibers and varying concentrations of granite filler in a polyester matrix. It further employs TOPSIS for optimal material selection and a Genetic Algorithm for design optimization of a semi-trailer loading floor, aiming to develop a cost-effective, durable, and eco-friendly composite solution. This approach not only seeks to advance material performance but also promotes sustainable resource utilization by adding value to agricultural (sisal) and industrial (granite waste) byproducts, potentially fostering local economic development.

CHAPTER THREE

3 MATERIAL SELECTION AND MANUFACTURING PROCESS

3.1 Materials

3.1.1 Sodium Hydroxide

Sodium hydroxide (NaOH) was chosen for treating sisal fibers in this study due to several important considerations. Its strong alkaline properties allow it to efficiently remove lignin and other unwanted substances from the fibers, thereby enhancing their quality and performance. Furthermore, NaOH is a cost-effective and easily accessible chemical that is commonly used across various industries, making it a practical option for this application. Its proven effectiveness in fiber treatment is well-supported by existing research, and the process can be carefully managed by adjusting variables such as concentration, temperature, and treatment duration. With appropriate safety precautions in place, NaOH presents a reliable and safe choice for fiber treatment. As a result, commercially available sodium hydroxide was selected for use in this study.

3.1.2 Polyester

The choice of unsaturated polyester resin for fabricating sisal-reinforced composites is supported by several key reasons. Primarily, this type of resin is known to exhibit excellent compatibility with natural fibers like sisal, promoting strong interfacial bonding and improving the mechanical performance of the composite. Additionally, the resin was sourced from a local composite material supplier, ensuring both availability and a steady supply throughout the research. Its cost-effectiveness, compared to other resin systems, further reinforces its suitability for research purposes. Unsaturated polyester resin also offers favorable processing features such as low viscosity and rapid curing, which aid in the efficient impregnation of sisal fibers and enable the production of composites with desirable characteristics. Moreover, its widespread use and proven reliability in the composites industry—particularly in applications involving natural fibers—underscore its appropriateness for this study. Based on these considerations, unsaturated

polyester resin was obtained locally and used in the preparation of sisal-reinforced composite materials.

3.1.3 Sisal Fiber

The selection of sisal fibers for semitrailer loading floor applications presents numerous benefits. To begin with, the widespread cultivation of sisal plants ensures a consistent and easily accessible supply of fibers, particularly in northern Ethiopia. This local availability reduces reliance on expensive imports and promotes regional economic development. Furthermore, sisal fibers are notably lightweight, contributing to a reduction in vehicle weight. This decrease enhances fuel efficiency, leading to both cost savings and environmental advantages. The adoption of sisal fibers in such applications also holds the potential to boost the livelihoods of local communities in northern Ethiopia. As research continues and new applications are explored, the demand for sisal can grow, creating a sustainable market and a steady income source for local farmers. Overall, the accessibility, lightweight characteristics, and economic potential of sisal fibers make them a highly suitable material for use in loading floor production, supporting both fuel efficiency initiatives and the local economy. Consequently, sisal fibers were sourced from the areas surrounding Mekelle in the Tigray region of Ethiopia. The sisal plant and the extracted fibers are illustrated in *Figure* 3-1.

a) b)

Figure 3-1: (a) Sisal plant (b) sisal fibers.

3.1.4 Granit Powder

Granite powder was selected as a hybrid filler material alongside sisal fibers for automotive cross bar applications due to its numerous advantages in enhancing composite performance. As a naturally hard and durable mineral, granite powder significantly improves the stiffness, strength, and load-bearing capacity of the composite—key requirements for structural automotive components like cross bars. When combined with sisal fibers, this hybrid material offers a strong, lightweight, and efficient alternative to conventional materials. In addition to its mechanical benefits, granite powder exhibits excellent resistance to wear, corrosion, and environmental degradation, contributing to the long-term durability and reliability of the cross bar under demanding operating conditions. This enhanced performance ensures structural stability over time, reducing maintenance needs and the risk of component failure. Granite powder is also an economical and sustainable choice. It is widely available as a byproduct of stone cutting and polishing in the marble industry, making it a low-cost filler material. In this study, the granite powder was collected from local marble manufacturers, supporting the use of regional resources while minimizing material costs and environmental impact. Repurposing this industrial waste helps reduce landfill burden and promotes sustainable manufacturing practices. The hybridization of sisal fibers with granite powder not only improves mechanical and thermal properties but also contributes to vehicle weight reduction, enhancing fuel efficiency without compromising safety or strength. Overall, the use of locally sourced granite powder and natural sisal fibers provides a cost-effective, durable, and eco-friendly solution for manufacturing automotive cross bars.

Therefore, the granite powder used in this study was collected from local marble manufacturers, where it is generated as a byproduct during cutting and polishing processes. This approach not only ensures a readily available and cost-effective supply of the material but also supports sustainable practices by repurposing industrial waste. Utilizing granite powder from nearby sources further promotes the use of local resources, reduces transportation-related emissions, and contributes to the development of environmentally conscious composite materials for automotive cross bar applications.

.

3.2 Manufacturing Process

In this study, the manufacturing process for fabricating composite laminates is explained in the following sections. The production of composite materials involves various techniques and treatments.

3.2.1 Fiber Treatment and Preparation

The sisal fibers used in this study were manually extracted from locally collected sisal leaves. To enhance their properties, the fibers underwent treatment using sodium hydroxide (NaOH). A 6% weight diluted solution of sodium hydroxide was employed for treating the sisal fibers. The fibers were immersed in this solution for duration of 3 hours, as per the recommendation of [63]. Subsequently, the fibers were washed with water to eliminate any residual sodium hydroxide and left to dry at room temperature for a period of three days.

3.2.2 Sisal ply Preparation

The sisal fibers were initially cut into lengths of 300 mm and then manually arranged in a unidirectional orientation to ensure continuous fiber alignment. To maintain this configuration, the aligned fibers were placed between sheets of paper on both the top and bottom surfaces. To secure the alignment and prevent displacement during handling, the fiber-paper assembly was stitched together using a sewing machine. Following the stitching process, the papers were removed by immersing the fabric in water, which facilitated easy separation from the fibers. After paper removal, the sisal fiber fabric was dried in direct sunlight for three days to ensure complete moisture evaporation. The outcome of this process was a fully dried, continuously aligned unidirectional sisal fiber fabric, as illustrated in *Figure* 3-2. This fabric served as the foundational reinforcement material for the subsequent preparation of composite laminates.

Figure 3-2: Unidirectional continuous sisal plies made by sewing.

3.2.3 Matrix Preparation

Firstly, the polyester resin was precisely weighed using a digital balance. Granite powder was then added to the resin at weight percentages of 2.5%, 5%, 7.5%, and 10%, and mechanical stirring equipment was used to thoroughly mix the filler and resin, ensuring a uniform and consistent dispersion while preventing agglomeration. The filler loadings were kept below 10% based on previous studies indicating maximum performance at these levels [35,36]. Once a homogeneous mixture was achieved, the required amount of Butanox hardener was carefully measured and added to the modified matrix, then mixed for an additional 2 minutes to ensure proper incorporation. The resulting granite-filled polyester matrix was subsequently used in the fabrication of the composite laminates. *Figure 3-3* shows the materials used for preparation of the matrix.

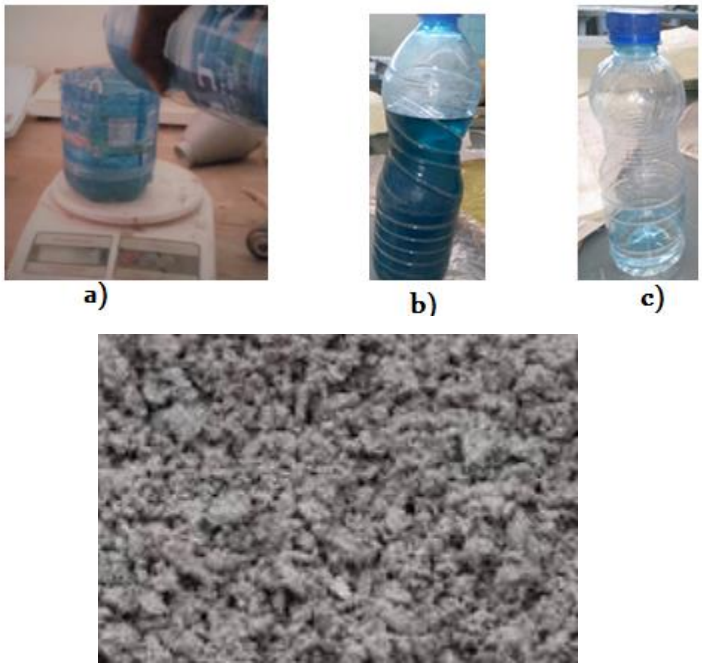

Figure 3-3: Matrix preparation: (a) weighing (b) polyester (c) hardener (d)granite powder.

3.2.4 Fabrication of Composite Laminates

The composites were fabricated using the hand layup method followed by compression molding. To facilitate easy removal of the cured composites from the mold, a releasing agent was applied beforehand. The sisal fiber content was selected based on previous studies, which identified 20 wt.% and 30 wt.% as the optimal levels [42,64]. Granite powder was incorporated as the filler material to evaluate its effect on the composites. Four different filler loadings—2.5 wt.%, 5 wt.%, 7.5 wt.%, and 10 wt.%—were used during fabrication. The matrix consisted of polyester resin, applied both in its pure form and modified with granite powder fillers. Two laminates, labeled S1 and S2, were prepared using the pure resin matrix combined with sisal plies, while the remaining sixteen composites (S3 to S18) were produced using the granite-modified resin matrix along with the sisal plies. During the fabrication process, the sisal plies were carefully positioned in the mold and impregnated by pouring the appropriate resin matrix over them. A roller was then used to ensure even distribution of the resin throughout the sisal layers and to remove any trapped air bubbles. The composites were cured under a constant load of 2 kN for 24 hours. Each composite measured 300 × 300 mm². The detailed composition of the composites, including the

amounts of sisal fibers, granite filler, and polyester resin, is presented in Table 3.1***Error! Reference source not found.***. Moreover, the manufacturing process is given in Figure 3.4.

Table 3.1: Composition of composites.

Laminate	Composition		
	Sisal (wt.%)	Polyester (wt.%)	Granite (wt.%)
E1	20	80	0
E2	30	70	0
E3	20	80	2.5
E4	20	80	5
E5	20	80	7.5
E6	20	80	10
E7	30	70	2.5
E8	30	70	5
E9	30	70	7.5
E10	30	70	10

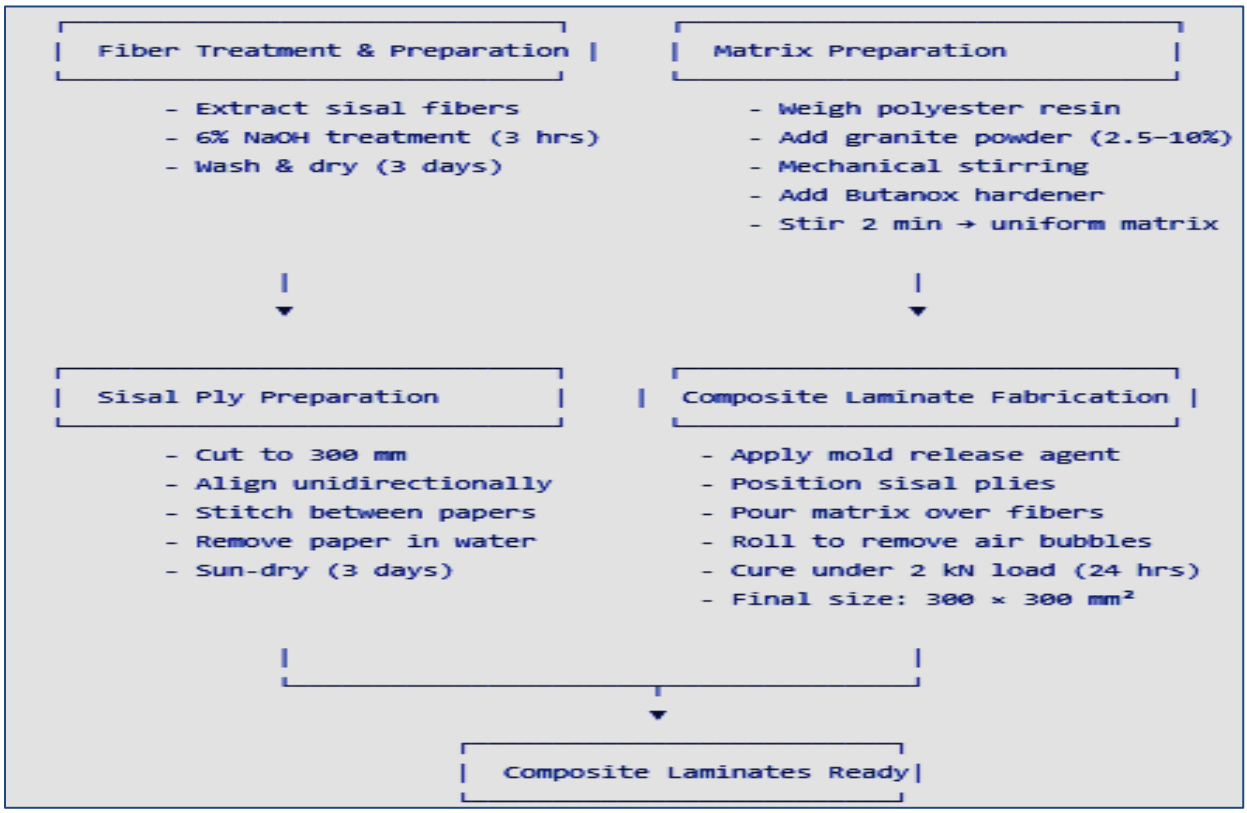

Figure 3-4: Manufacturing Process.

CHAPTER FOUR

4 EXPERIMENTAL METHODS AND ANALYTICAL PROCEDURES

4.1 Tensile Strength

Tensile test specimens were prepared following the ASTM D3039/D3039M [65] standard. To guarantee adequate sample size and statistical reliability, at least five specimens were cut from each laminate for testing. The specimens were precisely dimensioned at 250 × 15 × 3 mm^3. The ends of the samples were carefully polished using a file and emery paper to create smooth surfaces, removing any roughness or cracks that might influence the test outcomes. The tensile tests were carried out using a Microcomputer Controlled Electro-hydraulic Servo Universal Testing Machine, Model SI-1000KN, under ambient conditions. Testing was performed at a controlled crosshead speed of 2 mm/min to ensure consistent and accurate loading throughout the procedure.

4.2 Compressive Strength

Compressive testing was performed in accordance with ASTM D695-10 using rectangular specimens. Each specimen measured 12.7 mm × 12.7 mm in cross-section and 25.4 mm in length, maintaining the standard 2:1 length-to-width ratio. A total of five specimens were tested under ambient temperature conditions to ensure the reliability and repeatability of the results.

4.3 Impact Strength

Impact tests were conducted following the ISO 179–1[66] standard using a Charpy impact tester, specifically the Pendulum Impact Testing Machine, Model SI-42, with an impact energy of 150 J. For each test, at least five un-notched specimens measuring 80 × 10 × 4 mm^3 were prepared. During testing, the samples were struck by a hammer in both flatwise and normal orientations. The impact strength was determined by dividing the absorbed energy by the cross-sectional area of each specimen. All tests were performed under ambient conditions to ensure consistent testing environments and reliable, comparable results.

4.4 Flexural Strength

Flexural tests were carried out in accordance with ASTM D790-10 [67] using a Microcomputer Controlled Electro-hydraulic Servo Universal Testing Machine, Model SI-1000KN, the same machine used for the tensile tests. Specimens were prepared with dimensions of 125 × 13 × 3.2 mm^3, complying with the ASTM D790 standard. The tests employed a three-point bending setup, applying a constant loading rate until the specimens failed. During testing, the flexural strength was determined by examining the load-displacement data. This strength corresponds to the maximum stress the specimen endured at the point of failure. The highest load recorded immediately before fracture was used to calculate the flexural strength, typically expressed in force per unit area. All tests were conducted under ambient conditions to ensure consistent and reliable results.

4.5 Water Absorption

The water absorption behavior of the composite laminates was evaluated following the ASTM D570-98 [68] standard. Test specimens measuring 76.2 × 25.4 × 4 mm were prepared as per the standard specifications. Before the water absorption test, the specimens were dried in an oven at 50°C for 24 hours to ensure they were completely moisture-free. After drying, the samples were cooled to room temperature, and their initial weights were recorded using a digital balance with a precision of 0.01 g to establish a baseline for comparison. The specimens were then submerged in a water bath at room temperature and left to soak until fully saturated. Weight measurements were taken at predetermined intervals. Before each weighing, the specimens' surfaces were carefully dried with clean cotton to remove any excess water, and the measurements were recorded immediately to prevent environmental factors from influencing the results. The water absorption of the samples was calculated using Equation 4.1.

$$Ma = \frac{M_w - M_0}{M_0} x100\% \qquad 4.1$$

Where Ma is the percentage of water uptake the specimen, M_w is the weight of the wet specimen, and M_0 is the weight of the dry specimen.

4.6 Density

The density of specimens was determined following the ASTM D792-20 [69] standard. The specimens were prepared in accordance with the standard's specified dimensions. The mass of each specimen was measured using a precise balance with a precision of 0.01 g. The volume of the specimens was determined using displacement methods as outlined in the ASTM D792-20 standard. The density of the specimens was determined in units of mass per unit volume which provides valuable information about the material's compactness and mass distribution.

4.7 Performance Evaluation Using TOPSIS

4.7.1 Selection of Criteria for Evaluation

When developing an automotive component, multiple factors must be taken into account. Key considerations include tensile strength, impact resistance, flexural strength, compressive strength, material density, and water absorption. High tensile strength is essential for the component to endure significant loads without permanent deformation or breaking. Impact resistance ensures durability against sudden shocks and vibrations. Flexural strength is important for the component to retain its structural integrity under bending forces. Compressive strength enables the material to withstand pressure without collapsing. Lower density materials can reduce the overall weight, potentially enhancing fuel efficiency. Additionally, low water absorption is desirable to minimize the risk of corrosion and material deterioration. By thoroughly assessing these properties, the optimal material for the intended automotive application can be identified.

4.7.2 Weightage

In the material selection process for an automotive trailer floor, it is essential to assign appropriate weights to each evaluation criterion based on the specific performance requirements of the application. These weights are determined through expert judgment, taking into account the operational environment, expected mechanical loads, and long-term durability needs of the trailer floor. The goal is to reflect the relative importance of each property—such as tensile strength, impact strength, flexural strength, compressive strength, density, and water absorption—in meeting the demands of real-world use. To facilitate objective evaluation and comparison, the assigned weights are normalized so that their total equals one. This ensures that

the contribution of each criterion is proportionally represented when applying decision-making tools such as weighted scoring models or multi-criteria decision analysis (MCDA). For a trailer floor, which typically experiences heavy loading, repeated impact from cargo, flexural stresses during transit, and exposure to outdoor environmental conditions, certain material properties are especially critical. Impact strength and flexural strength receive higher weighting, as the floor must absorb dynamic loads and resist deformation under varying weight distributions. Compressive strength is also significant to prevent localized crushing under high loads. Tensile strength supports structural integrity, particularly when the floor is integrated with the trailer frame. Density plays a role in overall vehicle weight, which affects towing efficiency and fuel consumption. Water absorption must be minimized to reduce the risk of moisture-related degradation, especially when operating in wet or humid environments. The final weights assigned to each of these criteria, reflecting their relevance to the trailer floor application, are presented in Table 4.1. These weights provide the foundation for a systematic, performance-driven material selection process that ensures safety, reliability, and cost-effectiveness over the trailer's service life.

Table 4.1: Weight assignment for decision criteria.

Criteria	Tensile Strength	Compression Strength	Flexural Strength	Impact Strength	Water Absorption	Density
Weight =1	0.18	0.18	0.21	0.21	0.10	0.12

4.7.3 Calculation of Performance Scores using TOPSIS

TOPSIS (Technique for Order of Preference by Similarity to Ideal Solution) is a decision-making method used to rank alternatives based on their similarity to an ideal solution. It is commonly used when multiple criteria need to be considered in selecting the best alternative. The steps involved in the TOPSIS procedure are as follows:

Step 1: Construct a decision matrix that compares the performance of each alternative with respect to each criterion in matrix form as expressed in Table 4.2.

Table 4.2: Decision matrix.

Composites	Tensile Strength (Mpa)	Compression Strength (Mpa)	Flexural Strength (Mpa)	Impact Strength (KJ/m^2)	Water Absorption (%)	density (g/cm)
E1	70.14	54.08	103.11	94.23	6.2	1.4
E2	85.1	62.11	116.23	118.45	6.7	1.39
E3	80.45	63.65	109.25	119.87	5.6	1.41
E4	85.76	68.12	120.43	137.23	4.7	1.42
E5	95.76	72.79	130.15	152.12	3.8	1.43
E6	90.42	69.34	121.13	136.12	3.3	1.44
E7	99.98	68.14	141.27	146.23	5.8	1.43
E8	107.9	76.19	150.76	176.73	5	1.45
E9	102.87	70.17	141.11	160.21	4.2	1.46
E10	99.08	67.87	137.18	139.13	3.8	1.47

Step 2: Normalize the matrix by dividing each value by the sum of the squared values in the same column as given in Equation 4.22.

$$Rij = \frac{X_{ij}}{(\sum_{i=1}^{m} X_{ij}^2)^{1/2}} \quad 4.2$$

Where i = 1, 2... , m and j = 1, 2, ..., n. and X – denote the decision matrix and R- denote the normalized decision matrix.

Step 3: The obtained normalized matrix is then converted into the weighted normalized decision matrix (V_{ij}) by multiply each element in the normalized decision matrix R by its respective weight in Table 4.3 using Equation 4.3. The weighted normalized decision matrix is given in Table 4.3.

$$V\_ij = R\_ij * W\_j \quad 4.3$$

Where i = 1, 2, ..., m and j = 1, 2, ..., n.

Table 4.3: Weighted normalized decision matrix.

Composites	Tensile Strength	Compression Strength	Flexural Strength	Impact Strength	Water Absorption	density
E1	0.043	0.046	0.054	0.045	0.039	0.037
E2	0.052	0.052	0.060	0.056	0.042	0.037
E3	0.050	0.054	0.060	0.057	0.035	0.037
E4	0.053	0.057	0.057	0.065	0.030	0.038
E5	0.059	0.061	0.063	0.072	0.024	0.038
E6	0.056	0.058	0.068	0.065	0.021	0.038
E7	0.062	0.057	0.063	0.069	0.036	0.038
E8	0.066	0.064	0.073	0.084	0.031	0.038
E9	0.063	0.059	0.078	0.076	0.026	0.039
E10	0.061	0.057	0.073	0.066	0.024	0.039

Step 4: Determine the positive and negative ideal solutions: Identify the best and worst values among all alternatives for each criterion. The positive ideal solution is denoted as A+ and the negative ideal solution is denoted as A-. The positive ideal solution and the negative ideal solution of all the criteria are given in Table 4.4.

$$A+\_j = \begin{cases} \max(V\_ij), \text{if j is a benefit criteria or larger} - \text{the} - \text{better} \\ \min(V_{ij}), \text{if j is a cost criteria or smaller} - \text{the} - \text{better} \end{cases}$$

$$A-\_j = \begin{cases} \min(V\_ij), \text{if j is a benefit criteria or larger} - \text{the} - \text{better} \\ \max(V\_ij), \text{if j is a cost criteria or smaller} - \text{the} - \text{better} \end{cases}$$

Table 4.4: The positive ideal solution and the negative ideal solution.

S/N	Criteria	Ideal positive(A+)	Ideal negative (A-)
1	Tensile Strength	0.0665	0.0432
2	Compression Strength	0.0643	0.0456
3	Flexural Strength	0.0783	0.0535
4	Impact Strength	0.0840	0.0448
5	Water Absorption	0.0421	0.0208
6	Density	0.0390	0.0369

Step 5: Calculate the separation measures: The separation measures indicate how close or far an alternative is from the ideal solutions. Compute the Euclidean distance between each alternative and the positive ideal solution (D+) and the negative ideal solution (D-) using Equation 4.4. The results are given in Table 4.5.

$$D_i^+ = \sqrt{\sum_{j=1}^{n} \left(V_j^+ - V_{ij} \right)^2} \qquad 4.4$$

$$D_i^- = \sqrt{\sum_{j=1}^{n} \left(V_j^- - V_{ij} \right)^2}$$

Step 6: Calculate the relative closeness to the ideal solution: Determine the relative closeness (C) of each alternative to the ideal solution by calculating the ratio of the distance to the negative ideal solution and the sum of the distances to both ideal solutions using Equation 4.5. Thus, the alternative with the highest relative closeness value (C) is considered the best composite among the given alternatives. The relative closeness values (C) of all alternatives along with their ranks are given in Table 4.5. Based on the analysis presented in Table 4.5, composite E8 has emerged as the most appropriate material choice for the trailer floor application. This conclusion is drawn from its highest relative closeness value, which indicates superior performance in comparison to the other evaluated alternatives. The selection is based on multiple criteria, including mechanical strength, durability, cost-effectiveness, and overall suitability for structural applications in transportation. Thus, composite E8 is chosen not only for its favorable evaluation metrics but also for its potential to enhance the performance and longevity of the trailer floor. Consequently, this material composition will be utilized in the subsequent stages of the project, including the structural design, design optimization, and finite element analysis (FEA), to ensure the development of a robust and efficient trailer floor system.

.

$$C_i = \frac{D_i^-}{(D_i^+ + D_i^-)} \qquad 4.5$$

Table 4.5: The separation measures, the relative closeness and rank of alternative laminates.

Composites	Separation measures		Closeness factor	Rank
	D+	D-	C+	
E1	0.058	0.004	0.059	10
E2	0.043	0.018	0.290	9
E3	0.041	0.019	0.315	8
E4	0.034	0.029	0.460	7
E5	0.021	0.041	0.656	4
E6	0.025	0.037	0.595	5
E7	0.028	0.035	0.557	6
E8	0.012	0.054	0.820	1
E9	0.012	0.049	0.811	2
E10	0.021	0.040	0.659	3

4.8 Design and Optimization of Bus Roof Panel

4.8.1 Design Parameters and Materials

The input parameters for the selected semitrailer model, which served as the reference vehicle in this study, are detailed in Table 4.6. Additionally, the material properties of the sisal/granite fiber-reinforced hybrid composite used in the design optimization process are provided in Table 4.7.

Table 4.6: Input data for the modified semi-tailor loading floor.

Name	Semi-Trailer
Payload (ton)	60
Tare-weight (ton)	12
King pin position from front board (mm)	1300
Rear overhang to center of quake (mm)	3450
Total length of the semi-trailer (mm)	13500
Total width of the semi-trailer (mm)	2502
Load carrying length of the semi-trailer (mm)	13400
Spring center (mm)	920
Gross combination weight (ton)	84
Gross combination length (m)	18.5

Table 4.7: Mechanical properties of sisal/granite hybrid composite.

Tensile Modulus along longitudinal direction, E1(GPa)	7.21
Tensile Modulus along Transverse direction, E2 (GPa)	3.12
Poison's ratio, V12	0.32
Poison's ratio, V21	0.14
Shear Modulus (G12) (GPa)	2.5
Longitudinal strength in tension, X_t (MPa)	107.9
Longitudinal strength in compression, X_c (MPa)	76.19
Transverse strength in tension, Y_t (MPa)	57.34
Transverse strength in compression, Y_c (Mpa)	32.12
Shear strength, S (MPa)	29.45

4.8.2 Local Calculation

In this study, the critical loading scenario involves a uniformly distributed load applied across the entire area of the semi-trailer's loading floor. The semi-trailer is structurally supported at two primary locations: the kingpin connection at the front, which links it to the tractor unit, and the

rear axle support points. This setup reflects realistic operating conditions where the payload is evenly distributed over the floor surface, as typically observed during transportation.

A payload of 60 metric tons was considered, corresponding to a gravitational force of:

$$60t = 60 \times 1000kg \times \frac{9.81m}{s^2} = 550{,}800N(550.8KN)$$

The tare weight of the semi-trailer, obtained from the existing MIE design report, was taken as 8 metric tons, which equates to:

$$8t = 8 \times 1000kg \times 9.81m/s^2 = 78{,}480N(78.48KN)$$

The total static load applied along the trailer floor is therefore:

Total load =78,480N+550,800N=629,280N (629.28KN)

This loading condition was used to evaluate the stress distribution, deflection characteristics, and structural performance of the proposed sisal/granite fiber-reinforced hybrid composite floor under realistic service conditions.

4.9 Mathematical modeling

Classical Laminate Theory (CLT) is applied to model the semi-trailer's composite loading floor, with key assumptions simplifying the analysis while accurately capturing the mechanical behavior of the laminated structure. This approach enables effective prediction of stiffness, stress distribution, and deformation under applied loads, making it suitable for evaluating the structural performance of the hybrid composite floor under operational conditions.

4.9.1 Bending moment analysis

According to established mechanical design principles and plate theory, the composite loading floor of the semi-trailer is modeled as a simply supported continuous rectangular plate spanning over three supports. For analytical purposes, the loading floor is represented as a rectangular plate of width 'b' and length 'a', corresponding to the full dimensions of the floor structure. Assuming a uniformly distributed load acting over the surface, the maximum bending moments in the longitudinal (Mx) and transverse (My) directions, as well as the maximum shear forces, are calculated using classical plate theory formulations, as shown in Equations 4.6. This modeling approach enables a simplified yet accurate prediction of structural behavior under service loads. The load distribution applied to the composite loading floor is illustrated in Figure 4.1.

$$M_X = \beta q l^2$$
$$M_Y = \beta_1 q l^2 \qquad 4.6$$
$$V_X = \gamma q l$$
$$V_Y = \gamma_1 q l$$

Where; Mx & M_y are bending moments in X and Y direction respectively.

Vx & V_y are shearing forces in X and Y direction respectively.

q= load per unit area

a= shortest span length

b= longest span length

$\beta, \beta_1, \gamma, \gamma_1$ are length to width ratio coefficient.

l = the smaller of spans a and b

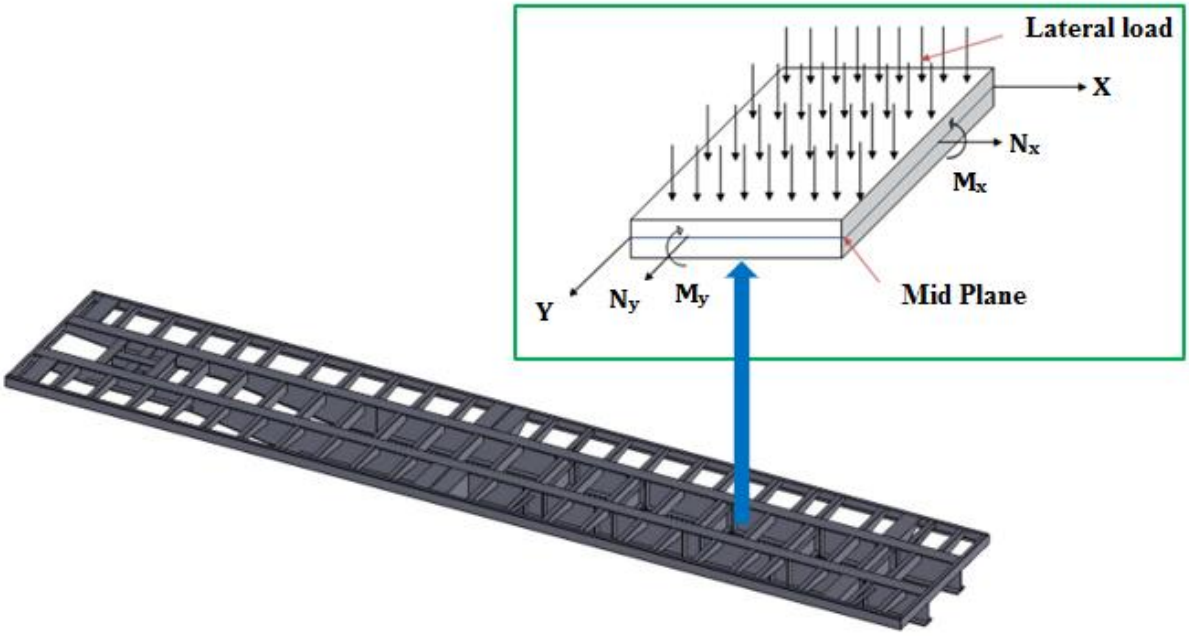

Figure 4-1: Load distribution of loading floor.

4.9.2 Stress-Strain Relationship

Hooke's Law is applied to analyze the stress distribution across the composite loading floor of the semi-trailer. Given the structural configuration and loading conditions, it is assumed that there are no significant out-of-plane forces acting on the floor. As a result, the loading floor can be idealized as a thin laminated structure subjected to in-plane forces only, justifying the use of the plane stress assumption. This simplification reduces the general three-dimensional stress–

strain relationships to a two-dimensional form, making the analysis more computationally efficient while maintaining accuracy. Under the plane stress condition, the composite laminate is treated as an orthotropic material, meaning its mechanical properties differ along different directions (e.g., fiber direction vs. transverse direction). Therefore, the stress–strain relationship is governed by the constitutive equations for orthotropic materials in two dimensions. These relationships are expressed in matrix form, as shown in Equation 4.7, and are fundamental to predicting how the laminate will deform under in-plane loading. This formulation is crucial for evaluating the structural response and optimizing the material layout of the composite loading floor under service conditions.

$$[\sigma_{ij}] = [Q_{ij}][\varepsilon_{ij}] \qquad i \; and \; j = 1, 2, 3 \ldots 6$$

$$\begin{Bmatrix} \sigma_1 \\ \sigma_2 \\ \sigma_3 \\ \tau_{12} \\ \tau_{13} \\ \tau_{23} \end{Bmatrix} = \begin{bmatrix} Q_{11} & Q_{12} & 0 & 0 & 0 & 0 \\ Q_{12} & Q_{22} & 0 & 0 & 0 & 0 \\ 0 & 0 & Q_{33} & 0 & 0 & 0 \\ 0 & 0 & 0 & Q_{44} & 0 & 0 \\ 0 & 0 & 0 & 0 & Q_{55} & 0 \\ 0 & 0 & 0 & 0 & 0 & Q_{66} \end{bmatrix} \begin{Bmatrix} \varepsilon_1 \\ \varepsilon_2 \\ \varepsilon_3 \\ \gamma_{12} \\ \gamma_{13} \\ \gamma_{23} \end{Bmatrix} \qquad 4.7$$

Since all the stress components in the Z-axis are zero due to the plane stress condition, the reduced stress-strain relationship for orthotropic materials is simplified to Equation 4.8.

$$\begin{Bmatrix} \sigma_1 \\ \sigma_2 \\ \tau_{12} \end{Bmatrix} = \begin{bmatrix} Q_{11} & Q_{12} & 0 \\ Q_{12} & Q_{22} & 0 \\ 0 & 0 & Q_{66} \end{bmatrix} \begin{Bmatrix} \varepsilon_1 \\ \varepsilon_2 \\ \gamma_{12} \end{Bmatrix} \qquad 4.8$$

Where, Q_{ij} is the reduced stiffness matrix that describes the elastic behavior of the ply under plane loading, given as follows:

$$Q_{11} = {E_1}/{(1 - v_{12}v_{21})}$$

$$Q_{12} = {v_{12}E_1}/{(1 - v_{12}v_{21})}$$

$$Q_{22} = {E_2}/{(1 - v_{12}v_{21})}$$

$$Q_{66} = G_{12}$$

Where:

E_1 - Longitudinal Young's modulus

E_2 - Transverse Young's modulus

v_{12}- Major Poisson's ratio

G_{12} - In-plane shear modulus

To evaluate the mechanical response of the semi-trailer's composite loading floor under applied loads, the mid-plane strains and mid-surface curvatures are calculated using the laminate stiffness matrix, commonly referred to as the ABD matrix. This comprehensive 6×6 matrix framework defines the relationship between the in-plane and out-of-plane loads applied to the laminate and the resulting strain and curvature responses. It encapsulates the overall elastic behavior of the composite floor by integrating the contributions of all individual plies across the laminate thickness. The ABD matrix is composed of three sub-matrices: [A], [B], and [D]. The [A] matrix represents the extensional stiffness, which relates in-plane forces to mid-plane strains. The [D] matrix captures the bending stiffness, relating applied moments to curvatures. The [B] matrix, known as the coupling stiffness matrix, describes the interaction between in-plane forces and out-of-plane bending — a phenomenon typical in unsymmetrical laminates. Together, these matrices provide a complete description of the laminate's stiffness characteristics. The relationship between the generalized loads (in-plane forces and bending moments) and the corresponding mid-plane strains and curvatures is mathematically represented by the ABD matrix formulation, as shown in Equation (4.9). This formulation is critical in analyzing and optimizing the performance of the composite floor under various load conditions, ensuring that the design meets the structural demands of real-world trailer operations.

Figure 4-2: Three-ply loading floor.

$$\begin{bmatrix} N \\ M \end{bmatrix} = \begin{bmatrix} [A] & [B] \\ [B] & [D] \end{bmatrix} \begin{bmatrix} \varepsilon^o \\ k \end{bmatrix} \qquad 4.9$$

As illustrated in Figure 4.2, the composite laminate used in the semi-trailer's loading floor is designed to be symmetric with respect to both geometry and material stacking sequence. In symmetric laminates, the bending–stretching coupling matrix [B] becomes zero, i.e., [B] = 0.

This eliminates any coupling between in-plane stretching and out-of-plane bending, thereby simplifying the structural analysis. The absence of coupling effects is advantageous for ensuring predictable and independent behavior under specific load cases. Since the composite floor is subjected primarily to a uniformly distributed transverse load, the structural response is dominated by bending rather than in-plane stretching. Under these conditions, the relationship between the applied loads and the resulting mid-plane strains and curvatures is simplified and governed by a reduced form of the laminate constitutive equation, as expressed in Equation 4.12. The global stress distribution in each ply of the laminate is determined using Equation 4.13, which calculates stresses based on the mid-plane strains and curvatures induced by the applied moments and forces. These deformation quantities are, in turn, derived using the extensional stiffness matrix [A] and the bending stiffness matrix [D], which are computed according to Equations 4.10 and 4.11, respectively. This analytical approach enables an accurate evaluation of internal stresses across the laminate's thickness, providing critical insight into the structural integrity and performance of the composite loading floor under service conditions.

$$A_{ij} = \sum_{k=1}^{n} \left[\bar{Q}_{ij}\right]_k (h_k - h_{k-1}), \qquad i,j = 1,2,6 \tag{4.10}$$

$$D_{ij} = \frac{1}{3}\sum_{k=1}^{n} \left[(\bar{Q}_{ij})\right]_k h_k^3 - h_{k-1}^3 \quad i \; and \; j = 1,2,6 \tag{4.11}$$

$$\begin{bmatrix} V_X \\ V_Y \\ 0 \\ M_x \\ M_y \\ 0 \end{bmatrix} = \begin{bmatrix} A_{11} & A_{12} & 0 & 0 & 0 & 0 \\ A_{12} & A_{22} & 0 & 0 & 0 & 0 \\ 0 & 0 & A_{66} & 0 & 0 & 0 \\ 0 & 0 & 0 & D_{11} & D_{12} & 0 \\ 0 & 0 & 0 & D_{12} & D_{22} & 0 \\ 0 & 0 & 0 & 0 & 0 & D_{66} \end{bmatrix} \begin{bmatrix} \varepsilon_x^0 \\ \varepsilon_y^0 \\ \gamma_{xy}^0 \\ k_x \\ k_y \\ k_{xy} \end{bmatrix} \tag{4.12}$$

$$\begin{bmatrix} \sigma_x \\ \sigma_y \\ \tau_{xy} \end{bmatrix} = \begin{bmatrix} \bar{Q}_{11} & \bar{Q}_{12} & \bar{Q}_{16} \\ \bar{Q}_{12} & \bar{Q}_{22} & \bar{Q}_{26} \\ \bar{Q}_{16} & \bar{Q}_{26} & \bar{Q}_{66} \end{bmatrix} \begin{bmatrix} \varepsilon_x \\ \varepsilon_y \\ \gamma_{xy} \end{bmatrix} \tag{4.13}$$

The $[\bar{Q}]$ reduced stiffness matrix is given in the following Equation 4.14.

$$[\bar{Q}] = \begin{bmatrix} \bar{Q}_{11} & \bar{Q}_{12} & \bar{Q}_{16} \\ \bar{Q}_{12} & \bar{Q}_{22} & \bar{Q}_{26} \\ \bar{Q}_{16} & \bar{Q}_{26} & \bar{Q}_{66} \end{bmatrix} \quad 4.14$$

Where

$$\bar{Q}_{11} = m^4 Q_{11} + 2m^2 n^2 (Q_{12} + 2Q_{66}) + n^4 Q_{22}$$

$$\bar{Q}_{12} = m^2 n^2 (Q_{11} + Q_{22} - 4Q_{66}) + Q_{12}(n^4 + m^4)$$

$$\bar{Q}_{22} = n^4 Q_{11} + 2m^2 n^2 (Q_{12} + 2Q_{66}) + m^4 Q_{22}$$

$$\bar{Q}_{16} = m^3 n (Q_{11} - Q_{12}) + mn^3 (Q_{12} - Q_{22}) + 2mn(m^2 - n^2) Q_{66}$$

$$\bar{Q}_{26} = mn^3 (Q_{11} - Q_{12}) + m^3 n (Q_{12} - Q_{22}) + 2mn(m^2 - n^2) Q_{66}$$

$$\bar{Q}_{66} = m^2 n^2 (Q_{11} + Q_{22} - 2Q_{12}) + (m^2 - n^2)^2 Q_{66}$$

Where $m = cos\theta \quad and \quad n = sin\theta$

The global strain in every ply can be calculated using the Equation 4.15 shown below.

$$\begin{bmatrix} \varepsilon_x \\ \varepsilon_y \\ \gamma_{xy} \end{bmatrix} = \begin{bmatrix} \varepsilon_x^0 \\ \varepsilon_y^0 \\ \gamma_{xy}^0 \end{bmatrix} + Z \begin{bmatrix} k_x \\ k_y \\ k_{xy} \end{bmatrix} \quad 4.15$$

Where ε_x^0 , ε_y^0 and γ_{xy}^0 represent the mid-plane strains and k_x , k_y and k_{xy} are the mid-plane curvatures, with z representing the distance from the mid-plane to the lamina (Figure 4.2). Stresses in the kth ply are analyzed using Equation 4.13, while principal stresses are obtained by applying the transformation matrix in Equation 4.16 to the stress matrix from Equation 4.13.

$$[T] = \begin{bmatrix} m^2 & n^2 & 2mn \\ n^2 & m^2 & -2mn \\ -mn & mn & m - n^2 \end{bmatrix} \quad 4.16$$

4.9.3 Optimization Using Genetic Algorithm

A Genetic Algorithm (GA) is employed to optimize the composite laminate configuration of the semi-trailer's loading floor, targeting minimum structural weight while maintaining sufficient load-bearing capacity and ensuring safety under operational conditions. In this study, all key

laminate parameters are treated as design variables, including the fiber orientation angles, individual ply thicknesses, and the stacking sequence. This comprehensive optimization allows the algorithm to explore a wide solution space to discover innovative, high-performance laminate designs. Each potential laminate configuration is encoded as a chromosome, where each gene represents a specific ply's orientation angle, thickness, and position in the stacking sequence. The GA evaluates these chromosomes using a fitness function that balances weight reduction with mechanical performance criteria. Structural integrity is enforced through the incorporation of the Tsai-Wu failure criterion, which ensures that no ply experiences failure under the applied transverse distributed loads. The fitness function also penalizes solutions that exceed allowable stress and strain limits, ensuring both safety and performance. The optimization process involves the core GA operators: selection, crossover, and mutation. Selection favors lighter, structurally compliant laminates; crossover combines features from high-performing designs to generate improved offspring; and mutation introduces small variations in ply properties or ordering to maintain diversity and avoid premature convergence. This iterative process, as depicted in the genetic algorithm flowchart in Figure 4.3, guides the evolution toward an optimal laminate layout. Classical Laminate Theory (CLT) is applied throughout the optimization to calculate the in-plane and bending stiffness matrices ([A], [D]), as well as the mid-plane strains and curvatures. These quantities are used to perform stress analysis for each ply, ensuring the design meets the mechanical demands imposed by the uniformly distributed payload. The stress results are checked against the Tsai-Wu criterion to verify structural safety at every step of the optimization. By optimizing all laminate parameters—orientation, thickness, and stacking sequence—the GA identifies non-intuitive, high-performance composite configurations that achieve significant weight reduction while maintaining or enhancing the structural integrity of the semi-trailer's loading floor. This approach not only improves vehicle efficiency and payload capacity but also provides a robust design methodology for advanced composite applications in transportation engineering

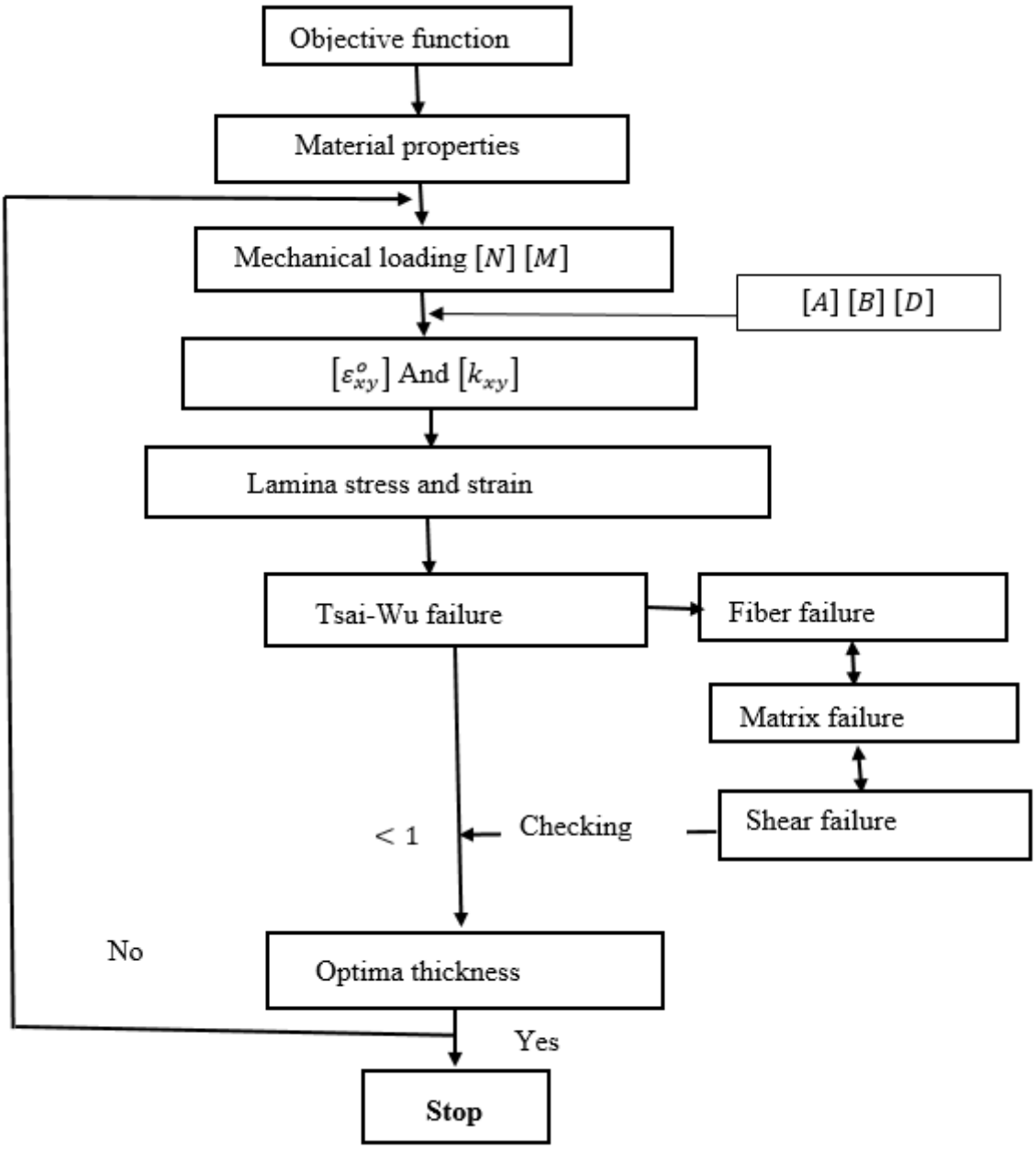

Figure 4-3:Flow chart for composite loading floor optimization using GA.

Objective function

The primary objective of optimizing the composite loading floor of the semi-trailer is to minimize its structural weight while maintaining its mechanical integrity under service loads. Accordingly, the objective function (F) is defined as the total weight of the laminate, which is to be minimized through the adjustment of key design variables—specifically, the fiber orientation angles, individual ply thicknesses, and stacking sequence. During the optimization process, the

Genetic Algorithm (GA) modifies these variables to reduce the overall weight of the floor panel, subject to constraints that ensure safe and reliable performance. One critical constraint is the Tsai-Wu failure criterion, which is applied to each ply to prevent material failure under the applied transverse distributed load. Additionally, stress and strain limits are incorporated into the design space to eliminate structurally infeasible configurations. Thus, the objective function for optimizing the composite loading floor can be mathematically represented as shown in Equation 4.17, where the total weight of the laminate is expressed as a function of the ply-level design variables. The optimization process seeks to identify a laminate configuration that minimizes this function while satisfying all mechanical and safety constraints imposed by loading conditions and material limits.

$$F(y) = Lb\rho(t1 + t2 + t3) \qquad 4.17$$

Where; L is length of the plate

b -Width of the plate

ρ -Material density

$t1, t2, t3$-Corresponding ply thickness of each composite material

Constraints and variables

In the Genetic Algorithm (GA) optimization process for the semi-trailer's composite loading floor, the Tsai-Wu failure criterion is employed as a critical constraint to ensure structural reliability and safety. This criterion is particularly suitable for composite materials as it accounts for both tensile and compressive failure modes, making it highly effective in capturing the complex failure behavior of fiber-reinforced laminates. The design variables considered in this optimization include the thicknesses of individual plies (t1,t2,t3) and their corresponding fiber orientation angles (θ1,θ2,θ3). These variables are systematically adjusted by the GA to minimize the total weight of the laminate while ensuring that the structural performance remains within allowable limits. To guarantee an adequate margin of safety under operational loading, a safety factor of 2 is applied within the Tsai-Wu failure criterion. This means the optimized design must not only avoid failure but must also demonstrate sufficient reserve strength under the worst-case loading conditions. By integrating this safety factor directly into the evaluation of each candidate solution, the GA filters out any configurations that approach critical failure thresholds.

The Tsai-Wu failure index is computed for each ply using the in-plane stress components resulting from the applied transverse distributed load. The simplified version of the Tsai-Wu failure criterion, as applied in this study, is expressed in Equation 4.18. This equation evaluates whether the combination of stress components and material strength parameters exceeds the allowable failure envelope for the laminate. This constraint ensures that the final optimized composite floor structure not only achieves minimal weight but also provides robust resistance to both bending and in-plane loads during service, thereby meeting the mechanical performance and safety requirements for real-world semi-trailer operations.

$$F_1\sigma_1 R + F_2\sigma_2 R + F_6\sigma_{12} R + F_{11}{\sigma_1}^2 R^2 + F_{22}{\sigma_2}^2 R^2 + F_{66}{\sigma_{12}}^2 R^2 + 2F_{12}\sigma_1\sigma_2 R < 1 \qquad 4.18$$

Where; $F_1, F_2, F_6, F_{11}, F_{12}, F_{66}\ and\ F_{22}$ are the components of the failure theory, σ_1, σ_2= principal stresses along the fiber and perpendicular to the fiber respectively, and R is the margin of safety.

4.9.4 Finite Element Analysis

The optimized composite loading floor design for the semi-trailer is validated using Finite Element Analysis (FEA) in ABAQUS to ensure the accuracy and practical feasibility of the Genetic Algorithm (GA) optimization results. This validation step compares the GA-derived laminate design with simulation outcomes to confirm that the optimized floor configuration meets structural performance expectations under real-world conditions. A structural model of the semi-trailer's loading floor is developed in ABAQUS using the optimized design parameters, including ply thicknesses, fiber orientations, stacking sequence, and geometric dimensions, all based on the GA results. The composite material used in this study is a sisal/granite fiber-reinforced polyester laminate, selected for its favorable mechanical properties and lightweight characteristics. The full laminate configuration is illustrated in Figure 4.4(a). The model is meshed using S4R shell elements with a 0.03 m mesh size to ensure sufficient accuracy in stress and deformation analysis. Boundary conditions are applied to represent the real-world supports—the floor panel is modeled as simply supported along all four edges, simulating attachment to the trailer chassis. A uniformly distributed static load, representing the combined payload and self-weight of the trailer, is applied across the floor surface, as shown in Figure 4.4(b). The FEA simulation calculates stress distribution and deformation under this applied load to assess the structural response of the optimized floor. The Maximum Stress Theory is used as

the failure criterion, evaluating the individual ply-level tensile, compressive, and shear stresses to ensure they remain within the allowable limits of the sisal/granite polyester composite material. By comparing the simulation results to design constraints, the FEA validation confirms whether the optimized design satisfies mechanical performance and safety requirements. This process ensures that the GA-derived laminate not only minimizes weight but also maintains sufficient structural integrity and durability under static service loads. All optimized configurations of the composite loading floor undergo this verification step to ensure they are structurally robust and suitable for real-world semi-trailer applications.

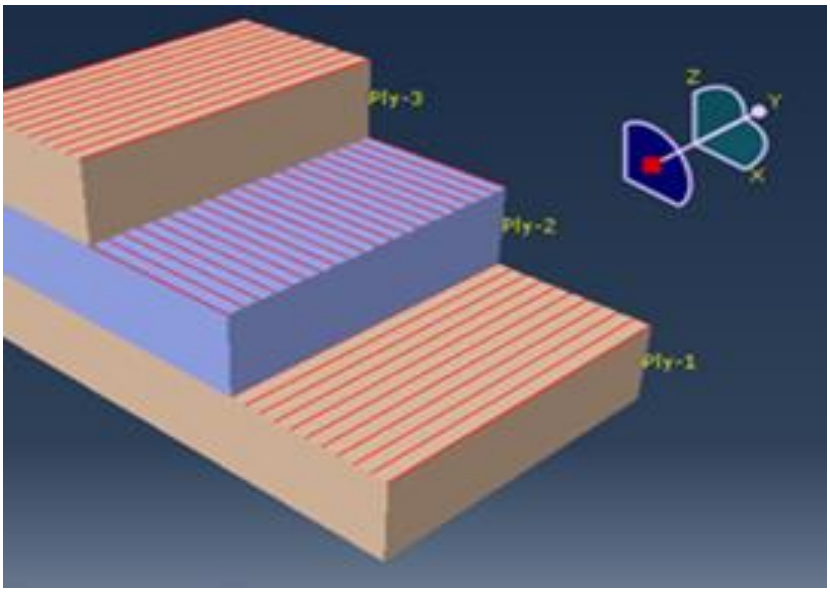

a)

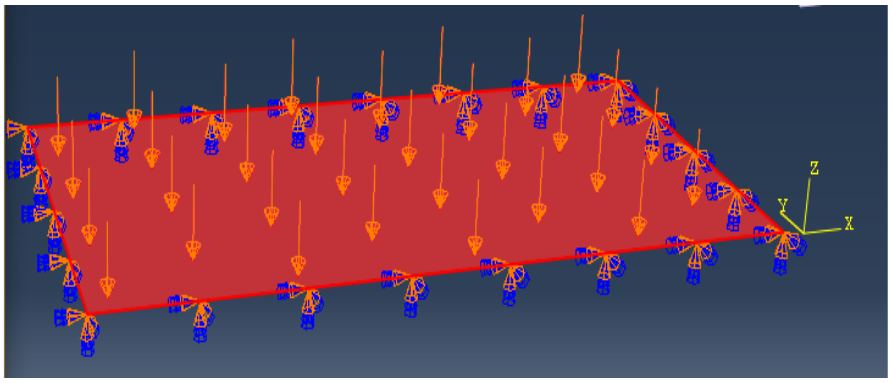

b)

Figure 4-4: Optimized loading floor: (a) Ply stacking sequence and orientation (b) Loading and boundary conditions.

CHAPTER FIVE

5 RESULTS AND DISCUSSION

5.1 Tensile Strength

Figure 5.2 provides valuable insights into the effect of granite powder on the tensile strength of sisal/polyester composites. The incorporation of granite particles led to a notable improvement in the tensile properties across both 20/80 and 30/70 fiber-to-matrix compositions. Among the 20/80 composites, the highest tensile strength was achieved with the inclusion of 7.5 wt.% granite (E5), whereas the 30/70 composites attained peak tensile strength at 5 wt.% granite addition (E8). This difference is primarily attributed to the higher resin content in the 20/80 composite, which allows for greater dispersion of granite fillers before issues such as agglomeration and interfacial weakening begin to reduce performance. In the 30/70 composites, the tensile strength began to decline beyond 5 wt.% granite due to the limited matrix content, which constrained proper distribution of the filler. The excess granite likely induced microstructural defects such as particle agglomeration, voids, or poor wetting, all of which degrade the interfacial bonding between the fibers, filler, and matrix [35,36,42]. The observed decrease after 5 wt.% suggests a critical filler loading threshold for maximizing mechanical efficiency without compromising the internal integrity of the laminate. Quantitatively, the 20/80 composites showed a maximum increase of 36.5% in tensile strength (from 70.14 MPa in E1 to 95.76 MPa in E5), while the 30/70 composites achieved a 26.7% improvement (from 85.10 MPa in E2 to 107.9 MPa in E8). Although the percentage gain was higher in the 20/80 configuration due to its lower initial strength, the absolute tensile strength was greater in the 30/70 composites. Notably, the 30/70 composite with 5 wt.% granite (E8) exceeded the tensile strength of all 20/80 samples, outperforming E5 by approximately 12.7%**.** This reinforces the importance of fiber content and filler dispersion synergy for optimizing mechanical performance. Therefore, based on the results, incorporating 5 wt.% granite powder into the 30/70 sisal/polyester composite is recommended to achieve superior tensile strength, offering the best balance between fiber reinforcement and matrix-filler interaction.

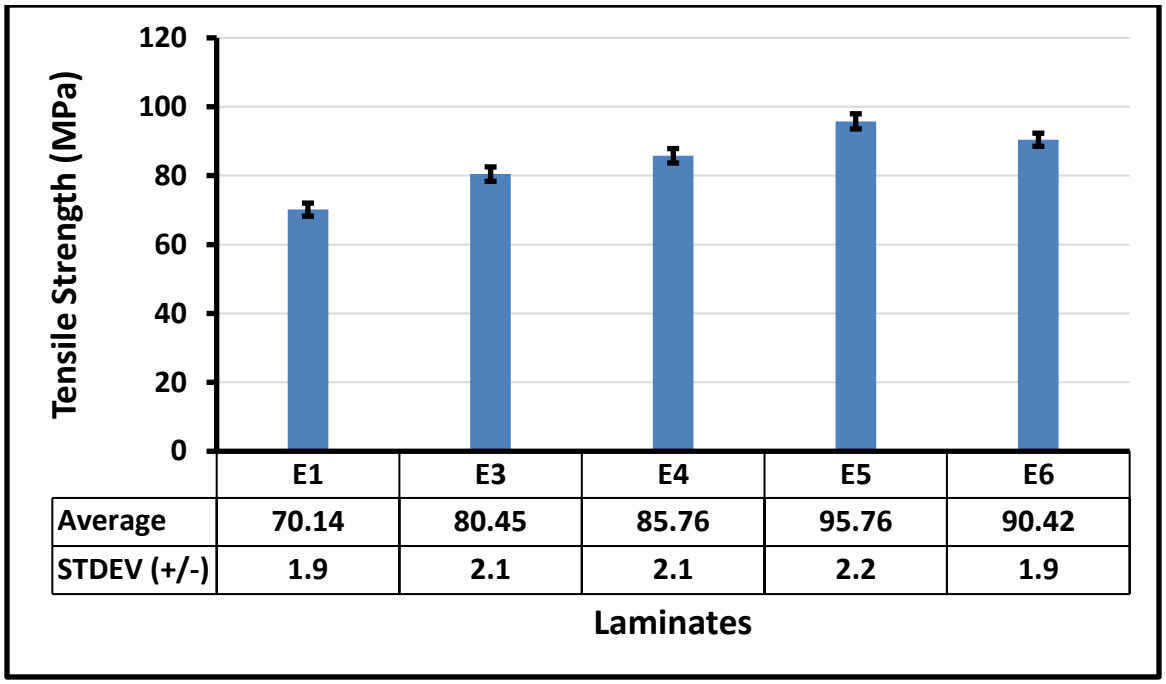

a)

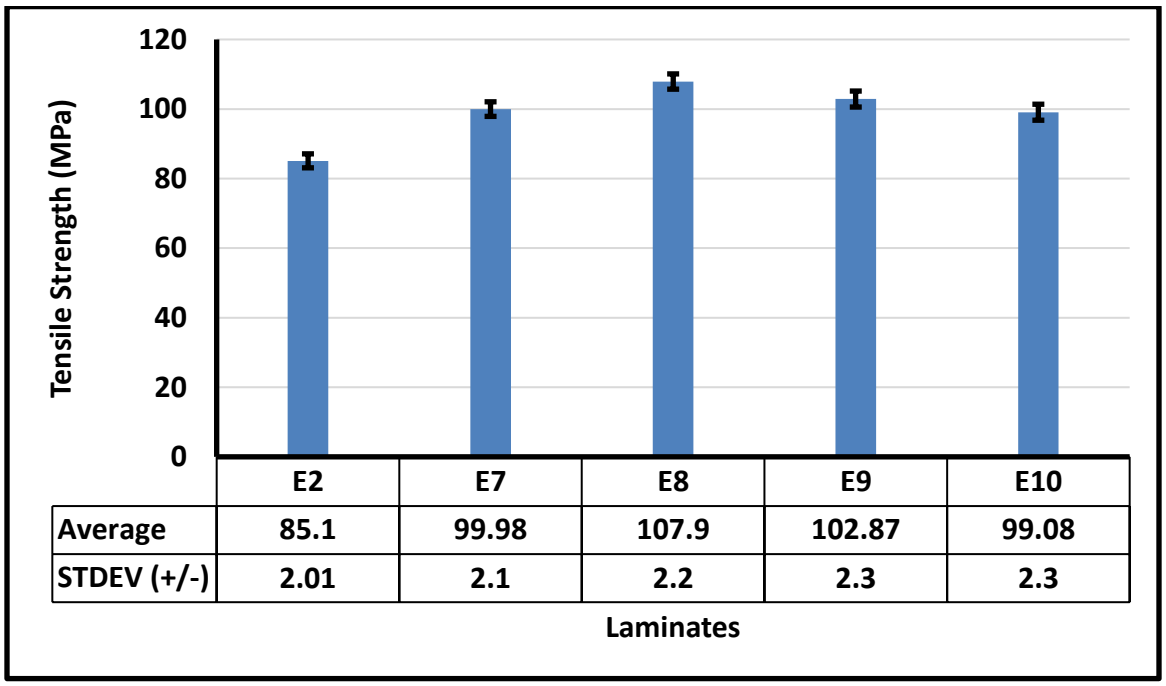

b)

Figure 5-1: Effect of granite fillers on tensile strength: (a) 20/80 composites and (b) 30/70 composites.

5.2 Compressive strength

Figures 5.2a and 5.2b depict the compressive strength behavior of sisal/polyester composites modified with varying granite powder contents. A consistent trend is observed across both laminate systems: compressive strength increases with filler addition up to an optimal level, beyond which a slight decline occurs due to filler-related issues. In the 20/80 fiber-to-matrix composites (Figure 5.2a), the inclusion of granite powder markedly enhanced compressive performance. The unmodified composite (E1) recorded the lowest strength at 54.08 MPa. Introducing 2.5 wt.% granite (E3) elevated the strength to 63.65 MPa, while the peak value of 72.79 MPa was achieved at 7.5 wt.% granite (E5)—representing a 34.6% improvement over the baseline. However, further increasing the granite content to 10 wt.% (E6) resulted in a slight reduction to 69.34 MPa, attributed to potential particle agglomeration, formation of resin-rich regions, and interfacial discontinuities that compromise the composite's structural integrity. A comparable trend was noted in the 30/70 composites (Figure 5.2b), which exhibited generally higher compressive strengths due to their greater fiber content. The control sample (E2) reached 62.11 MPa, which increased to a maximum of 76.19 MPa at 5 wt.% granite loading (E8), marking a 22.7% enhancement. However, beyond this point, compressive strength began to decline; the 7.5 wt.% formulation (E9) dropped to 70.17 MPa. This reduction can be linked to an insufficient resin matrix to adequately wet both the fibers and the increasing filler content, leading to microstructural defects such as voids, filler agglomerates, and poor interfacial adhesion. Overall, the results confirm that granite powder can effectively reinforce sisal/polyester composites when applied at optimal concentrations. For the 20/80 system, the optimal filler content is 7.5 wt.%, whereas for the 30/70 system, 5 wt.% granite yields the highest compressive strength. The greater improvement seen in the 30/70 composites suggests that increased fiber content enhances load distribution and stress transfer within the matrix. Nevertheless, maintaining an appropriate filler-to-matrix ratio is essential to avoid the adverse effects associated with overfilling. For applications where compressive strength is a key performance criterion, the 30/70 sisal/polyester composite with 5 wt.% granite powder offers the best balance between fiber reinforcement and filler enhancement. This composition provides optimal structural efficiency while minimizing defects related to excessive filler loading.

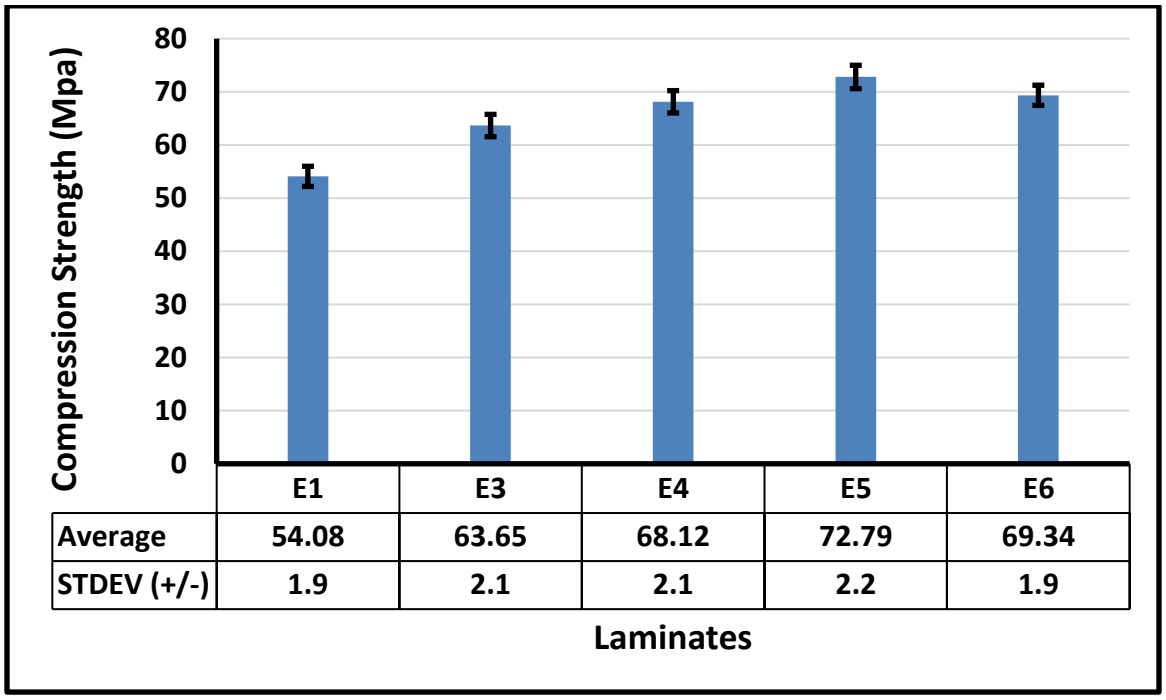

a)

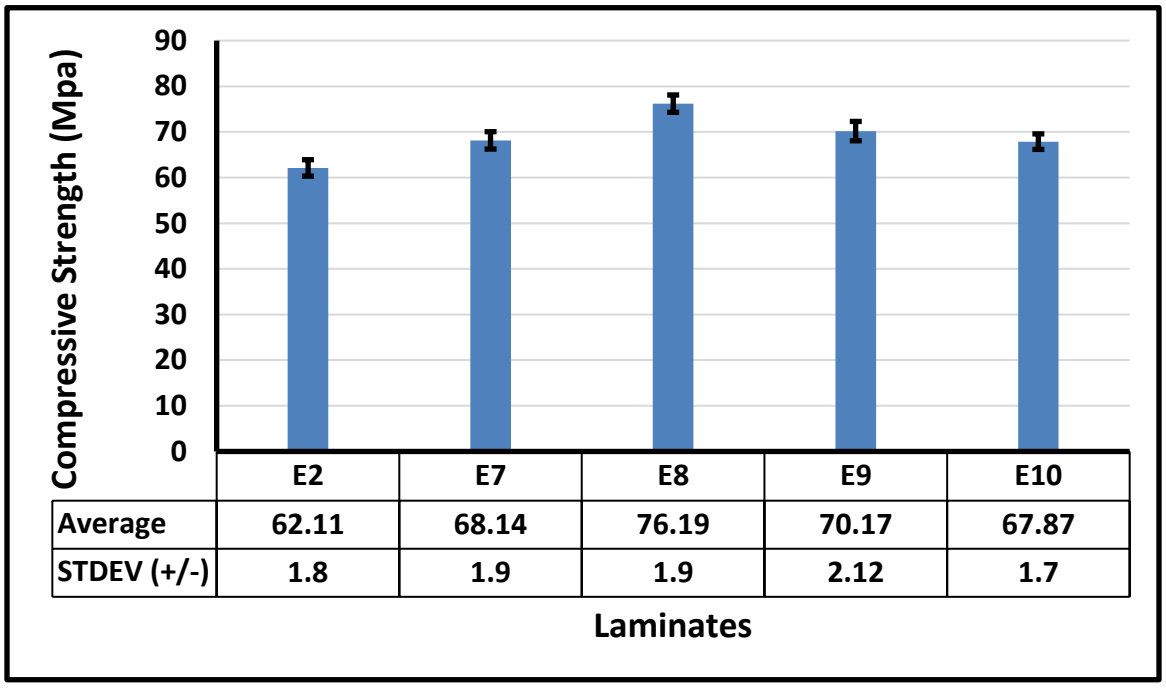

b)

Figure 5-2: Effect of granite fillers on compressive strength: (a) 20/80 composites and (b) 30/70 composites.

5.3 Flexural Strength

The provided bar graphs illustrate the flexural strength of sisal/polyester composites modified with varying weight percentages of granite powder, with Figure 5.3 a showing the results for the 20/80 fiber-to-matrix ratio composites and Figure 5.3 b depicting the 30/70 fiber-to-matrix ratio composites. A consistent trend emerges across both systems: the flexural strength generally increases with the addition of granite filler up to an optimal concentration, beyond which a slight decrease is observed, likely due to challenges associated with higher filler loadings. For the 20/80 sisal/polyester composites (Figure 5.3 a), the introduction of granite powder significantly influenced flexural strength. The unmodified composite (E1) recorded the lowest flexural strength at 103.11 MPa. Adding 2.5 wt% granite (E3) increased this to 109.25 MPa, while 5 wt% granite (E4) further improved it to 120.43 MPa. The peak flexural strength of 130.15 MPa was achieved with 7.5 wt% granite (E5), representing approximately a 26.2% improvement over the baseline. However, increasing the granite content to 10 wt% (E6) resulted in a slight reduction in strength to 121.13 MPa, potentially due to particle agglomeration, resin-rich areas, or interfacial defects. A comparable pattern was noted in the 30/70 sisal/polyester composites (Figure 5.3 b), which generally exhibited higher flexural strengths attributable to their greater fiber content. The control sample (E2) had a flexural strength of 116.23 MPa, which substantially rose to 141.27 MPa with 2.5 wt% granite (E7). The maximum flexural strength of 150.76 MPa was attained at a 5 wt% granite loading (E8), marking an enhancement of approximately 29.7% compared to the control. Beyond this point, the strength declined; the 7.5 wt% granite formulation (E9) dropped to 141.11 MPa, and the 10 wt% granite (E10) further decreased to 137.18 MPa, likely due to insufficient resin to adequately wet both fibers and the increasing filler, leading to microstructural imperfections. Overall, these results confirm that granite powder can effectively enhance the flexural strength of sisal/polyester composites at optimal levels: 7.5 wt% for the 20/80 system and 5 wt% for the 30/70 system. The superior performance of the 30/70 composites suggests better load-bearing capacity due to higher fiber content, though maintaining a proper filler-to-matrix ratio is crucial. For applications demanding high flexural strength, the 30/70 sisal/polyester composite with 5 wt% granite powder (E8) offers the most favorable balance of reinforcement and structural efficiency.

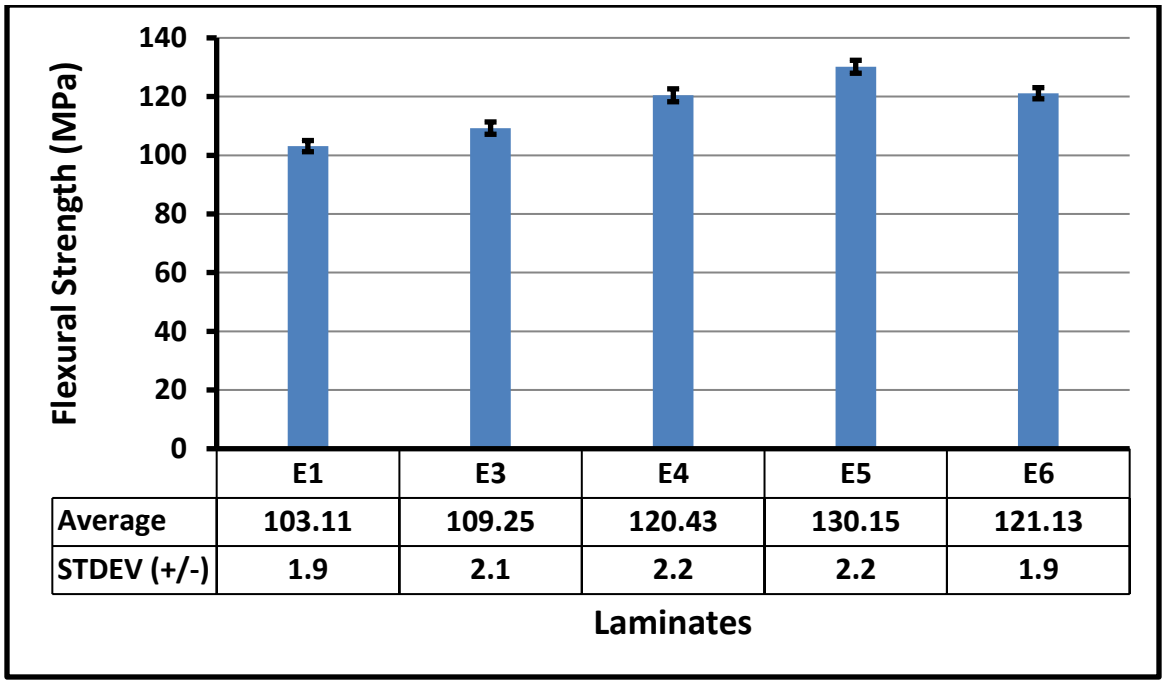

a)

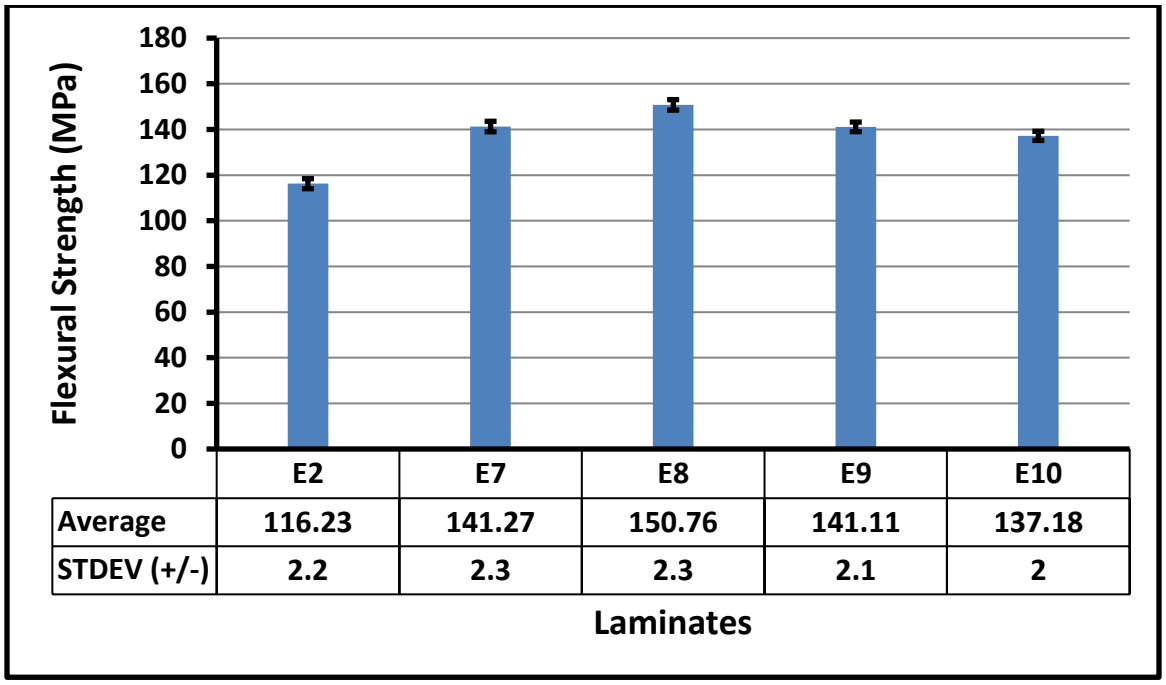

b)

Figure 5-3: Effect of granite fillers on flexural strength: (a) 20/80 composites and (b) 30/70 composites.

5.4 Impact Strength

The impact strength results of sisal/polyester composites modified with granite filler are presented in Figures 5.4a (20/80 fiber-to-matrix ratio) and 5.4b (30/70 ratio). Both systems exhibit a similar trend: impact strength initially increases with granite addition before declining at higher filler loadings, indicating an optimal reinforcement threshold. For the 20/80 composites (Figure 5.4a), the unfilled sample (E1) shows an impact strength of 94.23 KJ/m². The addition of 2.5 wt.% granite (E3) improves this by 27.2% to 119.87 KJ/m², while the 5 wt.% (E4) and 7.5 wt.% (E5) formulations achieve peak values of 137.23 KJ/m² and 152.12 KJ/m², respectively. However, at 10 wt.% (E6), the impact strength drops to 136.12 KJ/m², suggesting that excessive filler disrupts energy absorption. The 7.5 wt.% loading thus represents the optimal balance for this system. In the 30/70 composites (Figure 5.4b), the baseline impact strength (E2) is higher at 118.45 KJ/m² due to increased fiber content. The 2.5 wt.% (E7) and 5 wt.% (E8) granite loadings enhance this further to 146.23 KJ/m² and 176.73 KJ/m², respectively. Beyond 5 wt.%, performance declines, with the 7.5 wt.% (E9) and 10 wt.% (E10) samples dropping to 160.21 KJ/m² and 139.13 KJ/m². This confirms that the 30/70 system benefits most from 5 wt.% granite, as higher loadings likely cause resin starvation and poor filler dispersion. The superior impact resistance of the 30/70 composites underscores the reinforcing role of fibers, while the optimal filler thresholds (7.5 wt.% for 20/80 and 5 wt.% for 30/70) highlight the need to tailor filler content to the fiber-matrix ratio. These trends, illustrated in Figures 5.4a and 5.4b, emphasize that while granite filler enhances impact strength, its overuse can compromise performance due to agglomeration and interfacial defects. For applications demanding high impact resistance, the 30/70 composite with 5 wt.% granite is recommended, whereas the 20/80 system performs best at 7.5 wt.%.

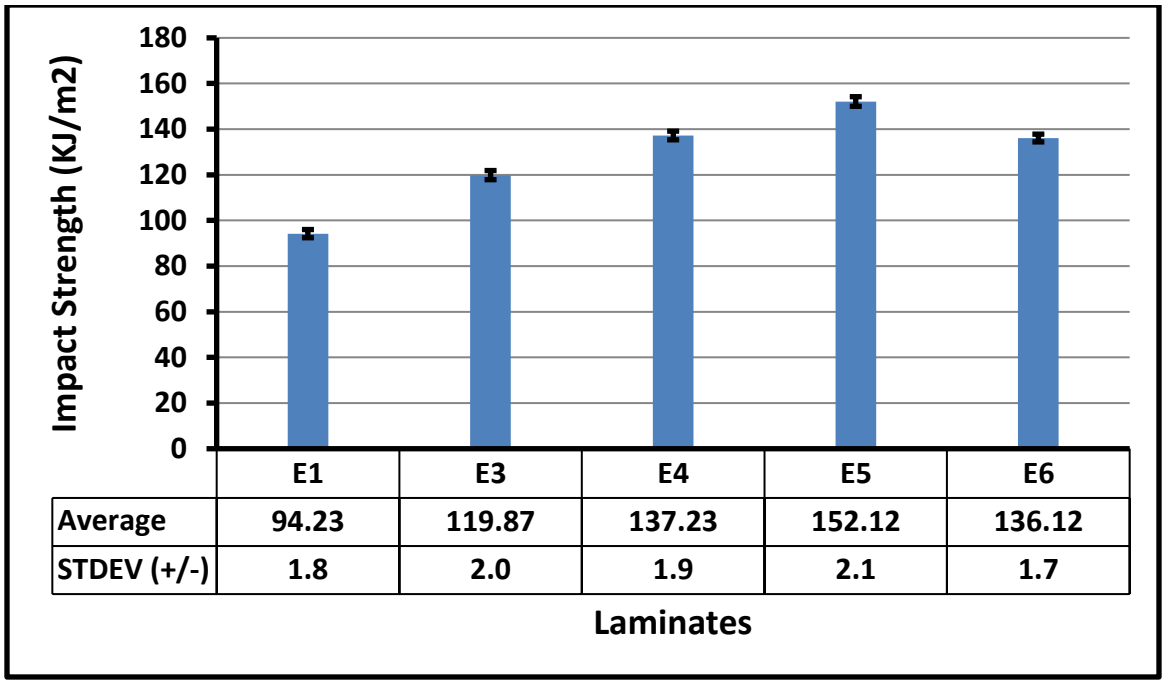

a)

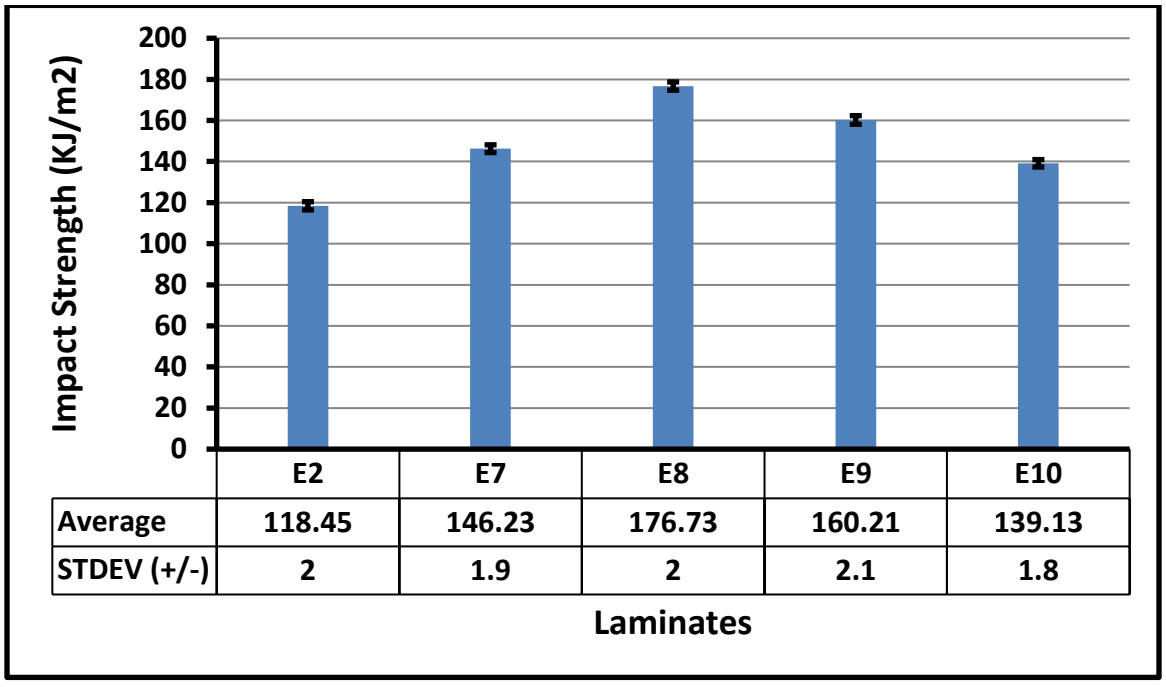

b)

Figure 5-4: Effect of granite fillers on impact strength: (a) 20/80 composites and (b) 30/70 composites.

5.5 Water Absorption

The water absorption behavior of sisal/polyester composites modified with granite filler, as detailed in Table 5.1 and Figures 5.5, reveals significant improvements in moisture resistance across both the 20/80 and 30/70 fiber-to-matrix ratio systems. In the 20/80 composite series, the unfilled laminate (E1) exhibited the highest water absorption at 6.2%, which progressively declined with increasing granite content—dropping to 3.8% at 7.5 wt.% (E5) and further to 3.3% at 10 wt.% (E6). A similar trend was observed in the 30/70 composites, where absorption decreased from 6.7% in the unfilled specimen (E2) to 4.2% at 7.5 wt.% (E9) and 3.8% at 10 wt.% (E10). These reductions correspond to relative decreases of 38.7–46.8% for the 20/80 system and 37.3–43.3% for the 30/70 system, clearly demonstrating the filler's effectiveness in enhancing hydrophobicity. The improved moisture resistance is attributed to several synergistic mechanisms. Granite particles act as impermeable barriers that inhibit water diffusion through the composite matrix. Their presence also enhances the overall density of the material, reducing microvoids and capillary pathways that typically facilitate water ingress. Additionally, the filler may partially shield the inherently hydrophilic sisal fibers, minimizing direct fiber exposure to moisture. This barrier effect is particularly effective up to 7.5 wt.%, beyond which the incremental gains in moisture resistance become marginal. Notably, while higher granite loadings (e.g., 10 wt.%) continue to reduce water absorption, they must be evaluated alongside mechanical performance, as excessive filler content has been shown to slightly reduce strength due to poor dispersion and interfacial issues. Therefore, 7.5 wt.% granite emerges as the optimal loading level, striking a balance between significant water absorption reduction (to 3.8% for 20/80 and 4.2% for 30/70 composites) and sustained mechanical integrity. From an application standpoint, these findings are particularly relevant for environments where dimensional stability and durability under humid or wet conditions are essential. While the 30/70 composites inherently absorb slightly more moisture due to their higher fiber content, their superior mechanical performance may offset this drawback in structural applications. In conclusion, granite filler not only improves the strength of sisal/polyester composites but also significantly enhances their durability by reducing moisture uptake.

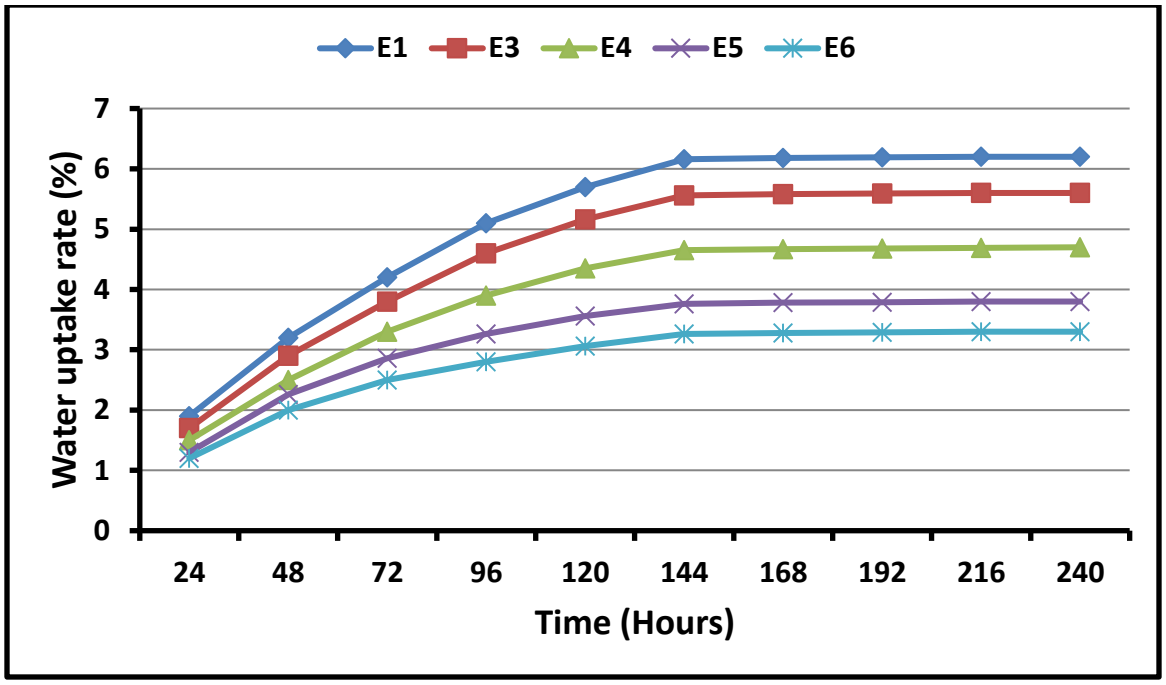

a)

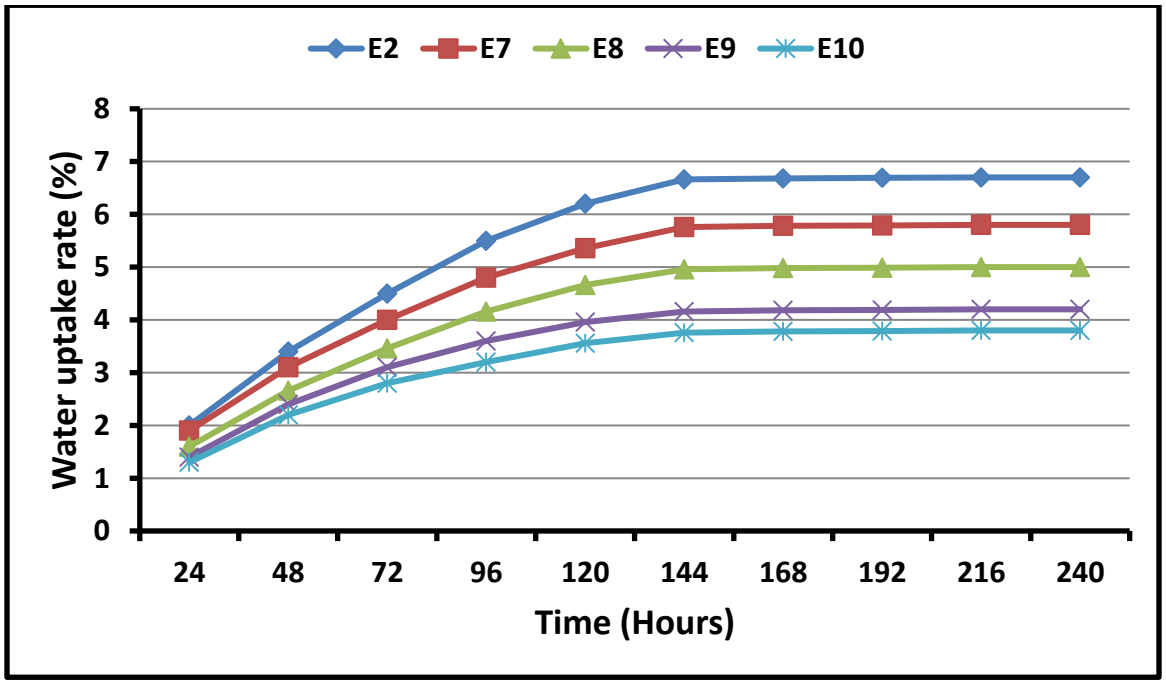

b)

Figure 5-5: Effect of granite fillers on water uptake rate: (a) 20/80 composites and (b) 30/70 composites.

Table 5.1: Percentage of water absorption at saturation.

Laminates	E1	E2	E3	E4	E5	E6	E7	E8	E9	E10
Average (%)	6.2	6.7	5.6	4.7	3.8	3.3	5.8	5	4.2	3.8
STDEV (+/-)	0.08	0.08	0.05	0.03	0.03	0.02	0.05	0.04	0.03	0.02

5.6 Density

The density measurements of the sisal/polyester composites provide valuable insight into the structural impact of granite filler incorporation. Across both the 20/80 and 30/70 fiber-to-matrix ratio systems, a consistent increase in density is observed with rising granite content as shown in Figure 5.6 a and b. This trend reflects the physical influence of the high-density filler on the composite's overall mass-to-volume ratio. In the 20/80 composites (E1–E6), density increases from 1.40 g/cm³ in the unfilled sample (E1) to 1.44 g/cm³ at 10 wt.% granite content (E6). A similar pattern is evident in the 30/70 composites (E2, E7–E10), where density rises from 1.39 g/cm³ in the control sample (E2) to 1.47 g/cm³ at 10 wt.% granite loading (E10). This systematic increase is primarily attributed to the higher specific gravity of granite particles compared to both the polyester matrix and sisal fibers. Several factors contribute to this enhancement in density. Firstly, granite's inherent density naturally raises the overall composite density when incorporated as a filler. Secondly, the filler particles assist in minimizing void content by filling gaps between the matrix and fibers, resulting in improved packing and a more compact microstructure. Furthermore, at optimal loading levels, granite particles may enhance fiber–matrix interfacial bonding, which further reduces the presence of microvoids and enhances structural cohesion. The observed increase in density aligns with other key improvements in composite performance. Higher-density samples—particularly those containing 5–7.5 wt.% granite, such as E5 and E8—also exhibited superior mechanical properties and reduced water absorption. Notably, the most significant density gains occur within the 0–5 wt.% filler range, beyond which the rate of increase tapers off, suggesting the system is approaching a packing limit where additional filler yields diminishing structural returns. In summary, the incorporation of granite filler contributes to the development of a denser, more tightly packed composite structure, which in turn supports enhancements in mechanical strength and moisture resistance. However, for applications where weight is a critical design factor, the increase in density must be

carefully balanced against the performance gains. The data demonstrate that moderate granite loadings offer the most efficient trade-off between improved composite properties and manageable weight increases.

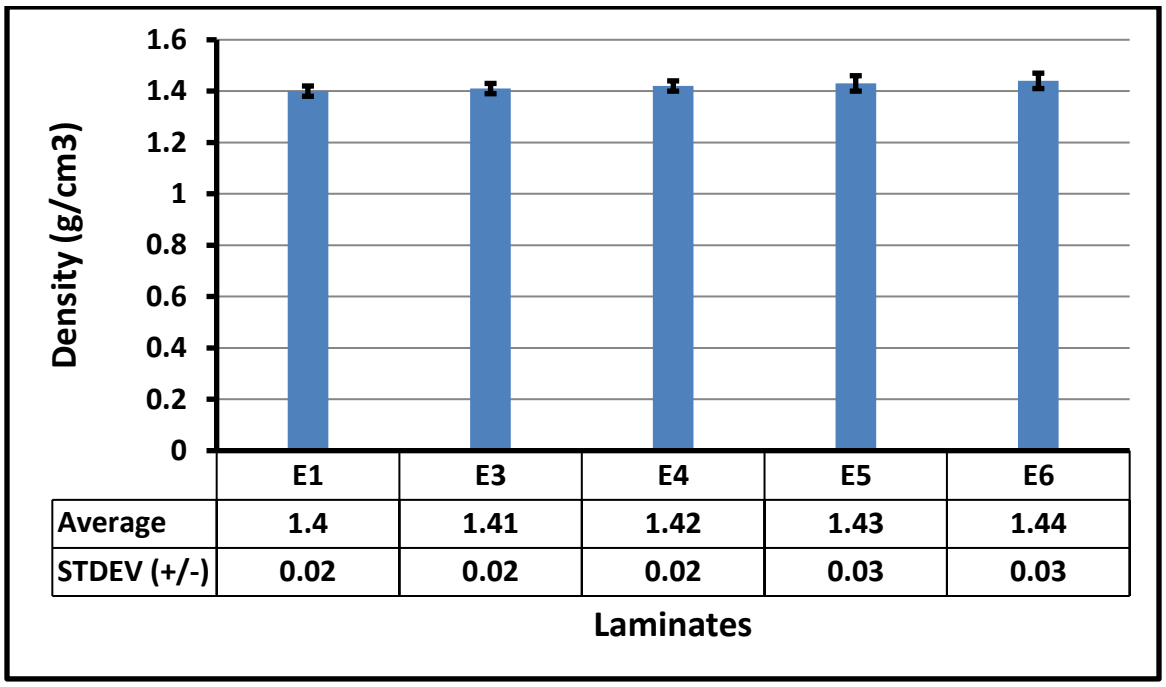

	E1	E3	E4	E5	E6
Average	1.4	1.41	1.42	1.43	1.44
STDEV (+/-)	0.02	0.02	0.02	0.03	0.03

a)

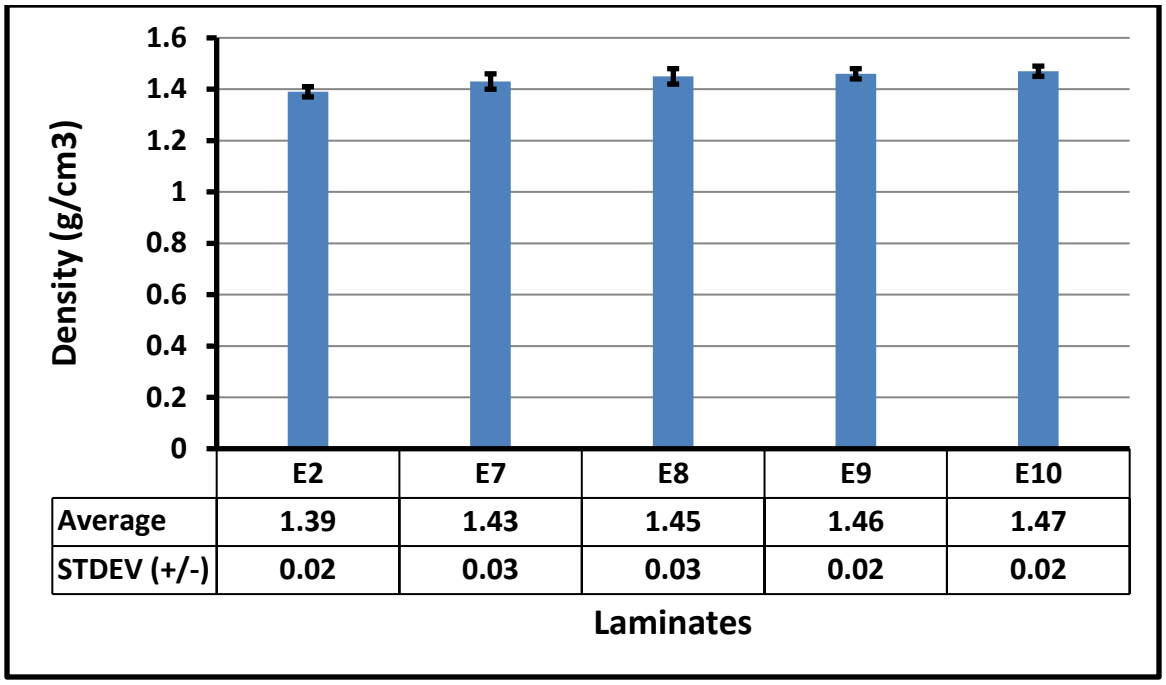

b)

Figure 5-6: Effect of granite fillers on density: (a) 20/80 composites and (b) 30/70 composites.

5.7 GA Optimization

Based on the results obtained from Genetic Algorithm (GA) optimization, composite materials are found to be preferable over conventional steel for the Semitrailer loading floor application, primarily due to their significant weight reduction. As shown in Table 5.2, the loading floor made from a hybrid sisal/granite composite weighs only 470.18 kg, compared to 1317.30 kg for its steel counterpart (Steel 52). This represents a substantial weight reduction of approximately 847.12 kg, or about 64.3%. Importantly, this reduction is achieved without compromising the load-carrying capacity or safety factor of the component, indicating the viability of composites as structural alternatives in transportation applications. This weight reduction has a direct impact on fuel efficiency. According to established data, for every 100 kg decrease in vehicle weight, fuel consumption is reduced by an average of 0.065 liters per 100 kilometers. Therefore, with a reduction of over 847 kg, the expected fuel saving is approximately 0.55 liters per 100 km. Over the course of 100,000 kilometers, this would result in a total fuel saving of around 550 liters. This has notable implications for fleet operations and logistics companies looking to reduce fuel costs and improve overall efficiency. Furthermore, reduced vehicle mass also contributes to

lower greenhouse gas emissions. It is estimated that fuel consumption and CO_2 emissions increase by about 6.5% for petrol engines and 7.1% for diesel engines with every additional 100 kg of mass. Thus, by replacing the steel loading floor with the hybrid composite version, a truck could avoid the emission penalties associated with such mass increases. In relative terms, this equates to avoiding up to 60.1% of the potential emission increases linked to the heavier steel component. The superior performance of the composite material can be attributed to several key advantages. First, the lightweight nature of natural and mineral fibers, such as sisal and granite, allows for a much lighter structure even with a slightly greater overall thickness (9.6 mm vs 5 mm for steel). Second, the use of a layered ply structure with a 0/90/0 orientation and ply thicknesses of 2.4 mm / 4.8 mm / 2.4 mm enables optimized mechanical performance. This balanced orientation enhances both longitudinal and transverse strength and stiffness, which is especially important for structural components like a loading floor that experience multi-directional loading. Third, from a sustainability standpoint, sisal is a renewable natural fiber, and granite particles can be sourced as an industrial by-product, making the composite both eco-friendly and cost-effective. In conclusion, the GA-optimized sisal/granite hybrid composite with a 0/90/0 ply orientation is a highly effective alternative to traditional steel for the semitrailer loading floor. It achieves remarkable weight reduction, significantly improves fuel efficiency, and contributes to lower CO_2 emissions, all while maintaining structural integrity and performance. These benefits underscore the growing importance and potential of natural fiber hybrid composites in the automotive and transportation sectors, particularly in the pursuit of lightweight, sustainable design.

Table 5.2: Comparison of GA optimized variables and objective function between steel and the hybrid sisal/granite composite loading floor.

Criteria	Sisal/granite hybrid composite	Steel 52
Weight (Kg)	470.18	1317.30
Orientation	$0^0/90^0/0^0$	n/a
Ply thickness t1,t2,t3 (mm)	2.4 4.8 2.4	5
Over all thickness (mm)	9.6	5
Width(mm)	2.502	2.502

5.8 Finite Element Analysis (FEA)

5.8.1 Stress

The structural performance of the sisal/granite hybrid composite loading floor was evaluated using Finite Element Analysis (FEA) in ABAQUS, with failure assessment performed using the Maximum Stress theory. The laminate is composed of three plies arranged in a 0/90/0 orientation, designed to provide balanced stiffness and strength in both longitudinal and transverse directions. The stress results for each ply—longitudinal (S_{11}), transverse (S_{22}), and shear (S_{12})—are presented in Table 5.3 and Figures 5.7 to 5.9. The outer layers (Ply 1 and Ply 3), aligned at 0°, bear the highest loads, exhibiting compressive and tensile stresses of ±18.42 MPa (S_{11}), ±14.66 MPa (S_{22}), and ±9.371 MPa (S_{12}). The middle layer (Ply 2), oriented at 90°, experiences significantly lower stress: –1.175 MPa (S_{11}), –0.198 MPa (S_{22}), and –1.223 MPa (S_{12}), as expected from its transverse orientation to the primary loading direction. Safety factors calculated using the Maximum Stress theory indicate that all plies are structurally sound, with values exceeding the failure threshold of 1. However, Ply 1 exhibits the lowest safety factor of 2.19 in the transverse direction, only slightly above the target safety factor of 2, which was set during genetic algorithm (GA)-based optimization using the Tsai-Wu failure criterion. While this confirms that the layer meets the design requirement, its proximity to the threshold identifies Ply 1 as the most critical layer under increased loading scenarios. This relatively low safety factor is not due to conservatism in the failure theory, but rather a result of actual mechanical vulnerability—particularly compressive stresses acting in both the fiber and transverse directions. Hybrid natural composites, such as sisal/granite, generally have lower compressive strength compared to tensile strength, making them more susceptible to failure mechanisms like matrix cracking or fiber micro-buckling under compressive loading. Therefore, Ply 1 is the most likely to initiate failure under load escalation. In contrast, Ply 2 exhibits exceptionally high safety factors—64.84 in the fiber direction and 162.2 in the transverse direction—attributed to its minimal stress exposure. Ply 3, which shares the same 0° orientation as Ply 1, undergoes a mirrored stress state but remains in tension, resulting in a slightly more favorable safety factor. In conclusion, the sisal/granite hybrid composite loading floor demonstrates robust structural performance, with all plies exceeding the minimum safety requirements. Nonetheless, Ply 1 remains the most vulnerable due to its compressive stress state, despite meeting the design threshold. This highlights the importance of considering compressive failure behavior in

laminate design and suggests that future improvements—such as targeted reinforcement, ply angle variation, or improved matrix properties—could further enhance performance and reliability under demanding loading conditions.

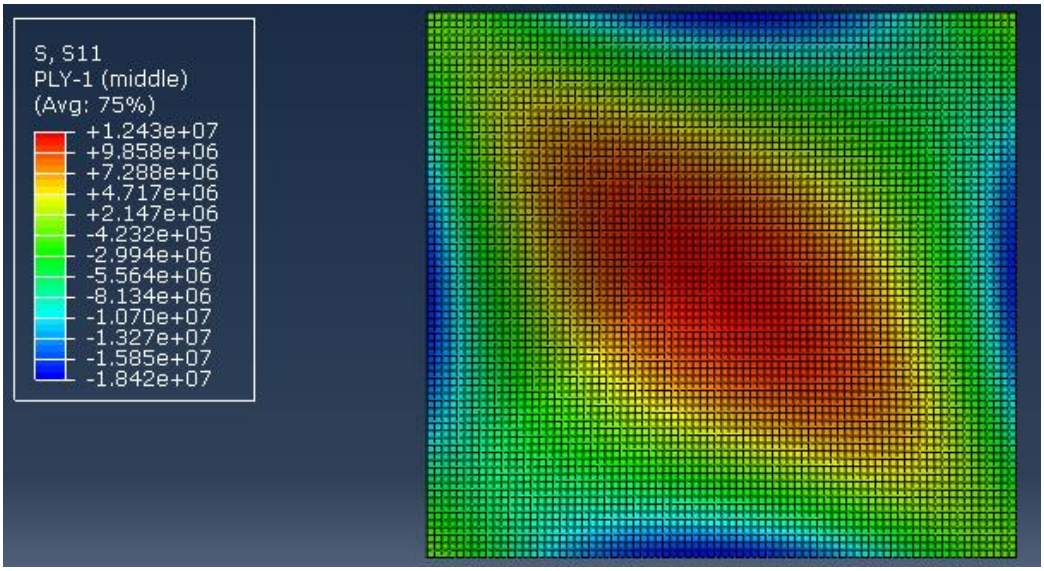

(a)

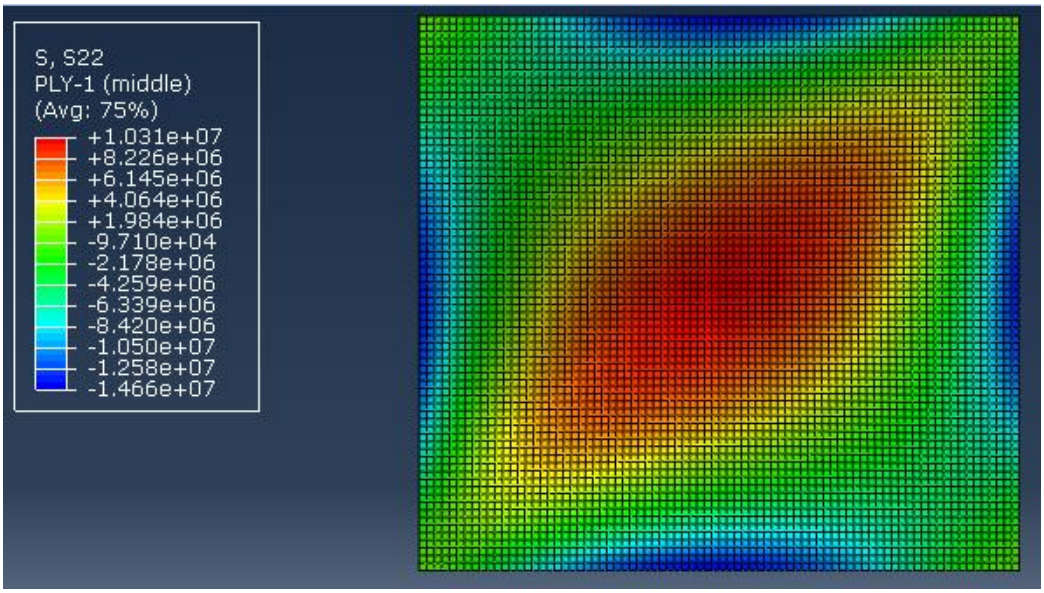

(b)

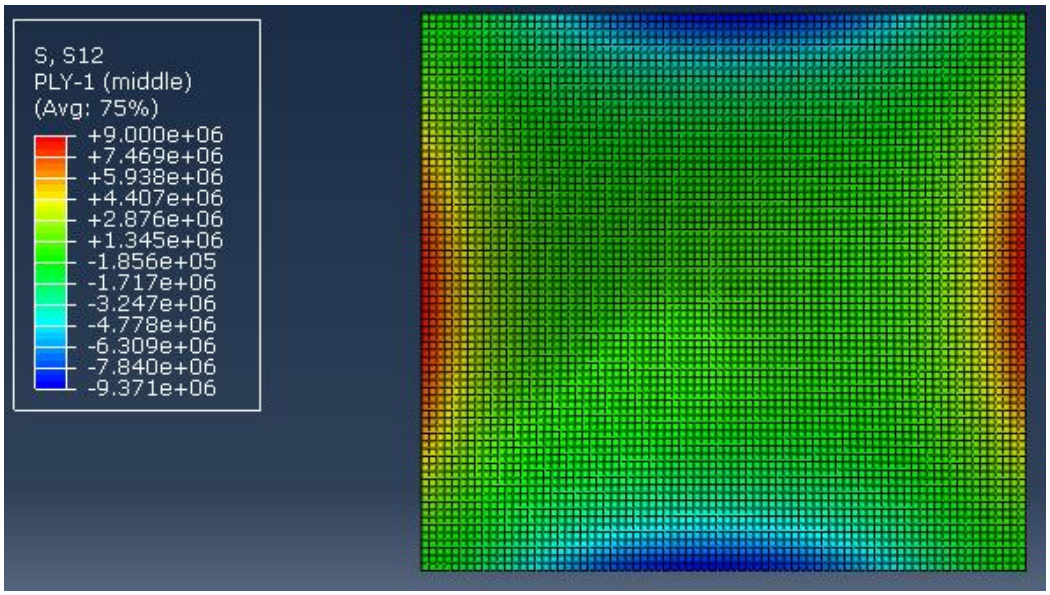

(c)

Figure 5-7: Ply-1 stresses (a) Longitudinal (S11), (b) transverse (S22), and (c) in-plane shear (S12).

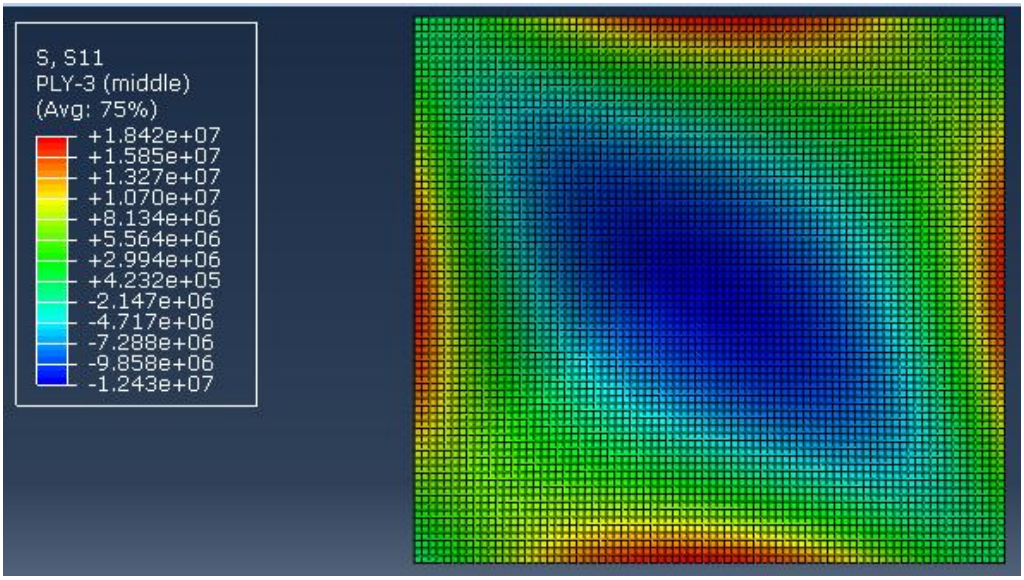

(a)

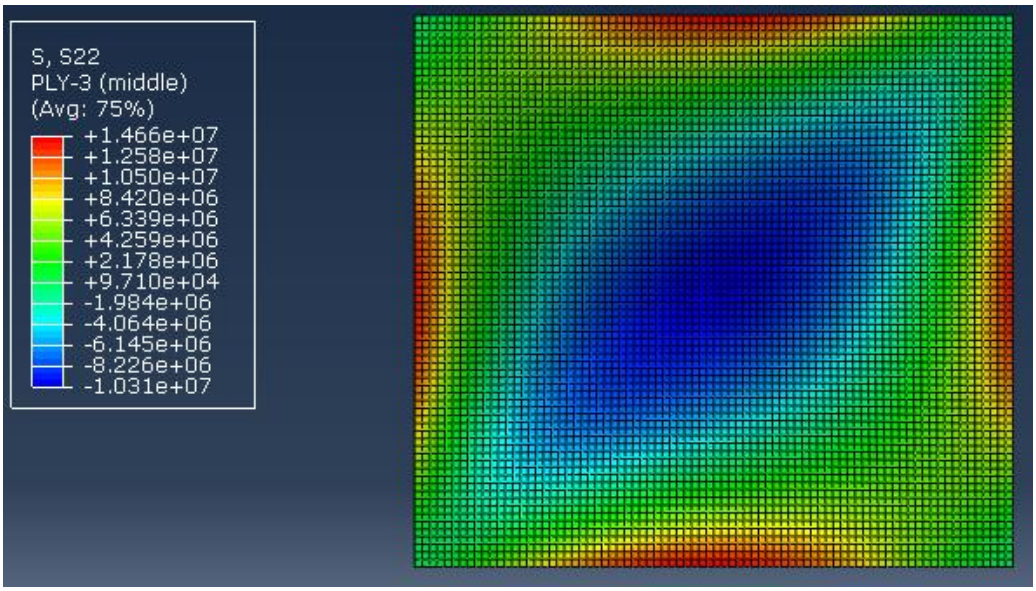

(b)

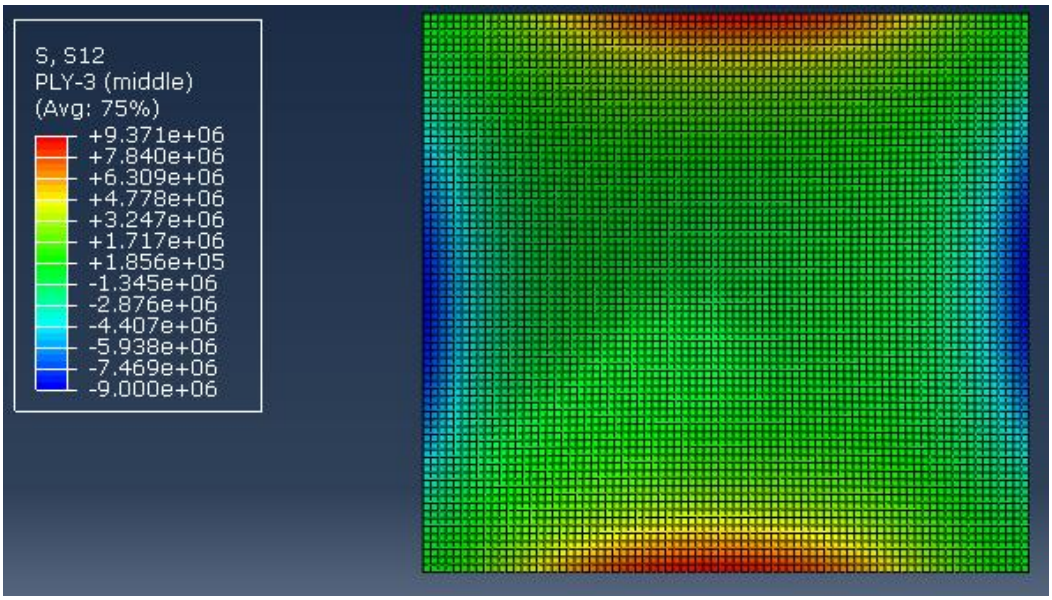

(c)

Figure 5-8: Ply-3 stresses (a) Longitudinal (S11), (b) transverse (S22), and (c) in-plane shear (S12).

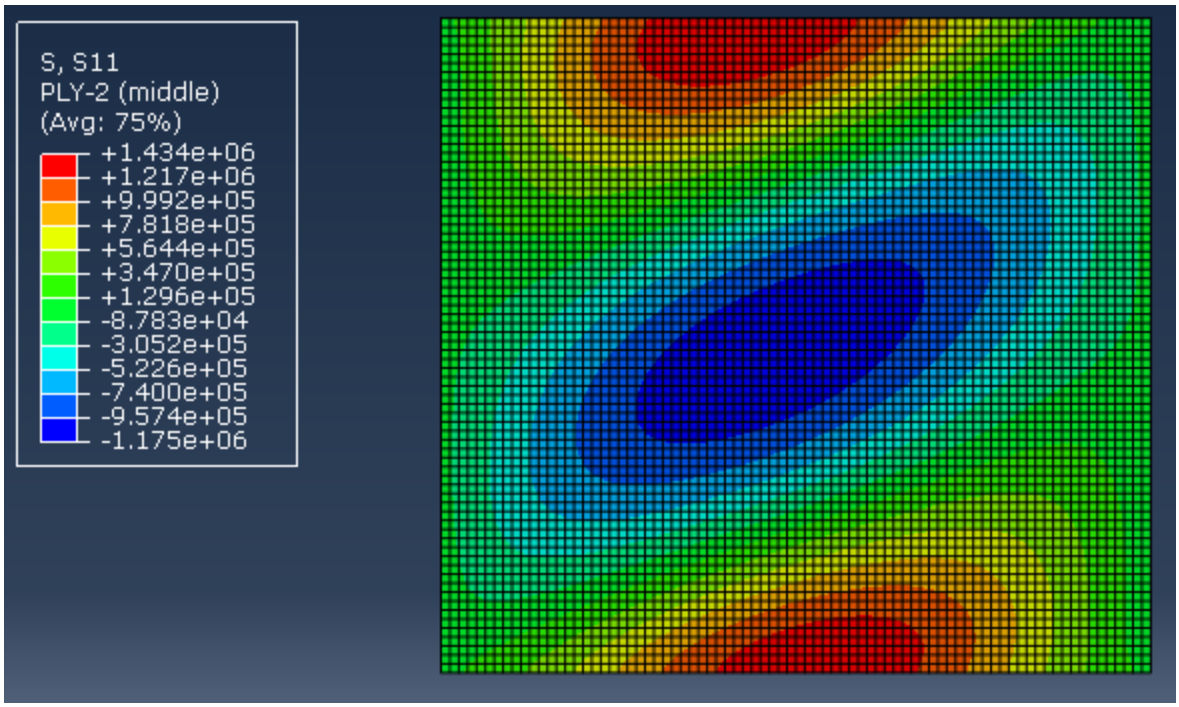
S, S11
PLY-2 (middle)
(Avg: 75%)
+1.434e+06
+1.217e+06
+9.992e+05
+7.818e+05
+5.644e+05
+3.470e+05
+1.296e+05
-8.783e+04
-3.052e+05
-5.226e+05
-7.400e+05
-9.574e+05
-1.175e+06

(a)

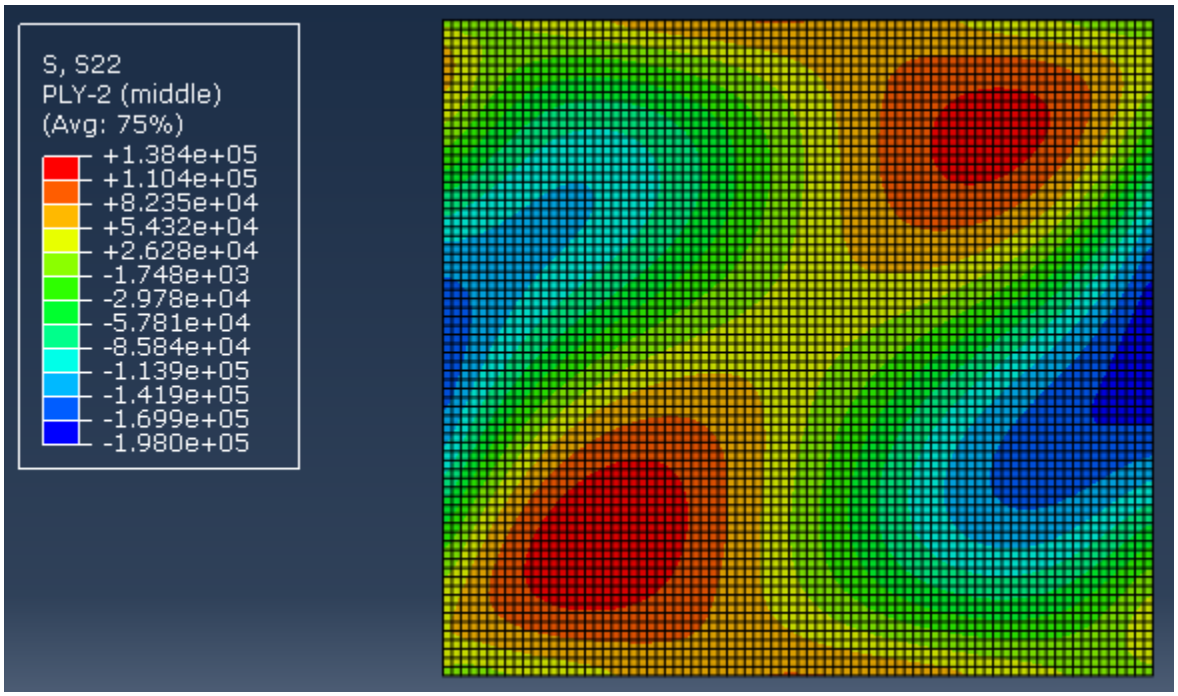
S, S22
PLY-2 (middle)
(Avg: 75%)
+1.384e+05
+1.104e+05
+8.235e+04
+5.432e+04
+2.628e+04
-1.748e+03
-2.978e+04
-5.781e+04
-8.584e+04
-1.139e+05
-1.419e+05
-1.699e+05
-1.980e+05

(b)

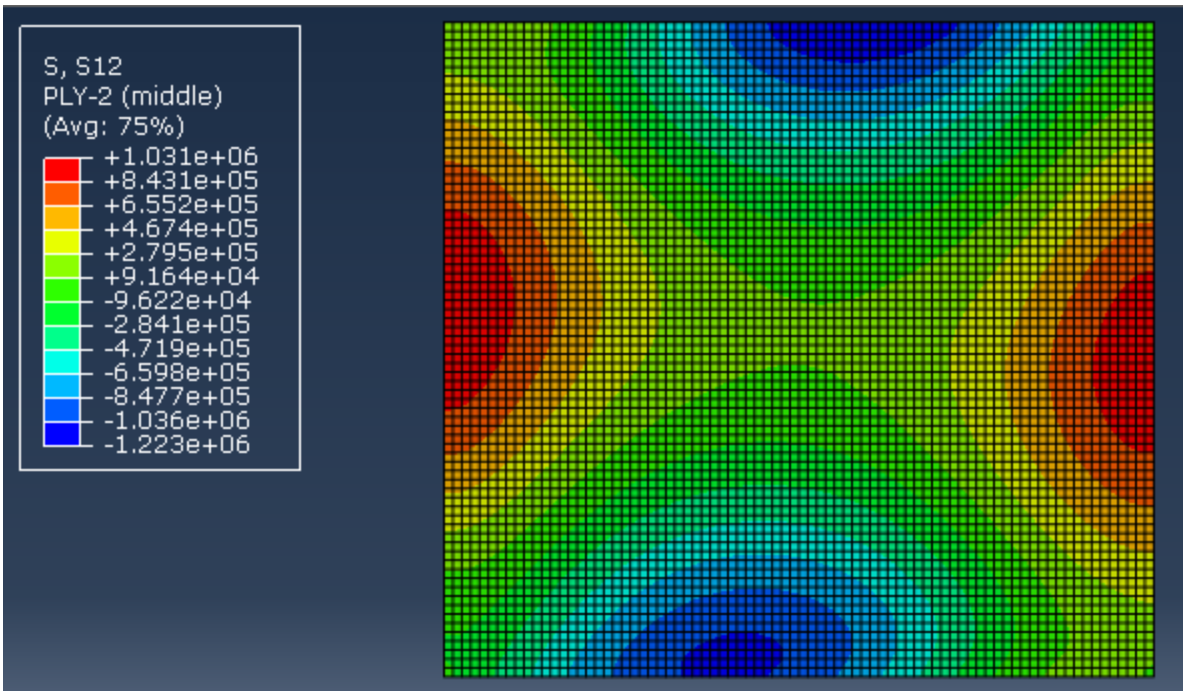

(c)

Figure 5-9: Ply-2 stresses (a) Longitudinal (S11), (b) transverse (S22), and (c) in-plane shear (S12).

Table 5.3: Stress distribution and safety factor along the cross-section of the semi-trailer loading floor.

Maximum stress		Sisal/granite hybrid composite		
		Ply1	Ply2	Ply3
S11(MPa)		-18.42	-1.175	18.42
S22(MPa)		-14.66	-0.198	14.66
S12(MPa)		-9.371	-1.223	9.371
Safety factor using Maximum Stress theory	1-direction	4.17	64.84	5.86
	2-direction	2.19	162.2	5.2
	Shearing	3.14	24.08	3.14

5.8.2 Deflection

Figure 5.10 illustrates the bending behavior of a sisal/granite hybrid composite laminate, evaluated as a potential material for semitrailer loading floors. The figure presents results from a

finite element analysis (FEA), depicting the displacement magnitude under applied loading. A color contour map is used to represent the deflection, with red indicating zones of maximum displacement and blue representing areas of minimal or zero deflection. This visual representation helps to understand the deformation pattern and the structural response of the laminate under load. The simulation reveals a maximum deflection of 1.459 mm, occurring at the center of the panel—where the structure is most susceptible to bending due to its distance from the supports. This central region is shown in red, indicating the highest deformation, while the outer edges, depicted in blue, remain largely undeformed due to being fixed or supported. Such a deflection pattern is typical of panels that are supported along their perimeter and experience either centrally applied or uniformly distributed loads, as would be the case in a semitrailer loading floor. To determine whether the deflection is within acceptable engineering limits, it is standard to compare the measured value against a deflection criterion such as L/300, where L is the unsupported span of the panel. In this case, the longest unsupported span is 850 mm, which means the allowable deflection is approximately 2.83 mm. Since the observed maximum deflection of 1.459 mm is well below this threshold, the composite structure can be considered sufficiently stiff for the intended application. This low level of deflection indicates that the laminate is capable of maintaining its structural integrity and supporting heavy loads without excessive deformation, which is essential for safe and reliable cargo transport. The use of a sisal/granite hybrid composite offers a desirable combination of sustainability and performance. Sisal fibers, being natural and renewable, provide lightweight reinforcement and good tensile strength. Granite particles enhance the laminate's compressive strength, stiffness, and wear resistance. Together, these reinforcements result in a hybrid material that is both strong and lightweight—qualities that are highly valuable in transportation systems where minimizing weight while maximizing durability is a key objective. Moreover, the smooth gradient of deflection from the center toward the edges suggests efficient load distribution and uniform stress handling. This even deformation behavior reduces the risk of localized stress concentrations, which can cause fatigue or failure over time. Such mechanical performance supports the long-term durability of the laminate, even under dynamic or repeated loading conditions typically encountered during freight operations. In conclusion, the sisal/granite hybrid composite demonstrates excellent mechanical performance for use in semitrailer flooring applications. The maximum deflection of 1.459 mm, remaining well within the allowable limit of

2.83 mm for an 850 mm span, confirms the material's structural adequacy. Its favorable balance of strength, weight, and durability, combined with the benefits of sustainability and efficient load management, make it a promising candidate for advanced transportation and infrastructure applications. Further refinement through simulation and material optimization can enhance its performance even further for demanding real-world conditions.

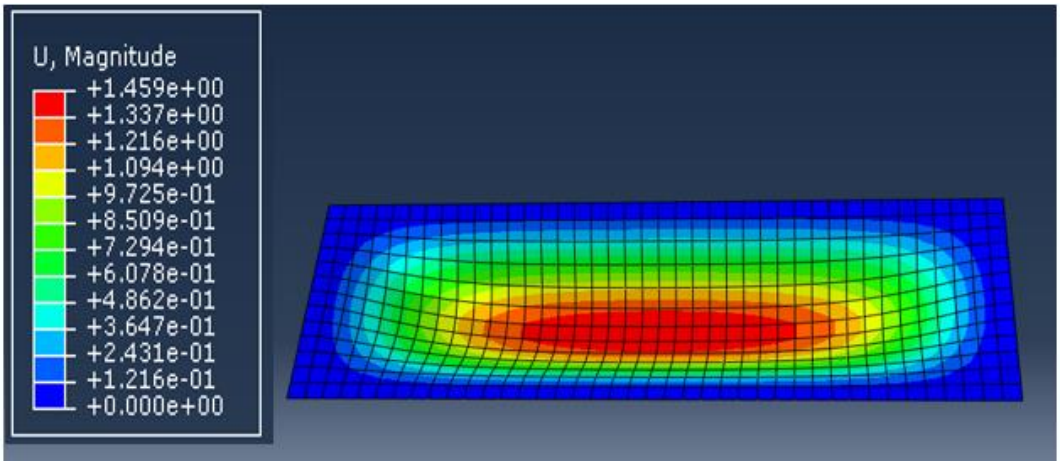

Figure 5-10: Deflection of the sisal/granite hybrid composite loading floor.

CHAPTER SIX

6 CONCLUSION AND FUTURE WORKS

6.1 Conclusion

This study investigated the development and optimization of sisal/granite hybrid composite laminates for use in semi-structural transport applications, specifically focusing on semi-trailer loading floors. The objective was to produce a lightweight, sustainable, and mechanically robust material using locally sourced alkali-treated sisal fibers and granite powder as reinforcement in a polyester matrix. Experimental results confirmed that incorporating 5 wt.% granite powder into a 30 wt.% sisal-reinforced polyester laminate (E8) yielded the most favorable balance of properties. This composite showed significantly enhanced mechanical strength, including tensile, flexural, compressive, and impact resistance, while also reducing water absorption by up to 43.3% compared to the unfilled system. This moisture resistance is crucial for structural panels subjected to variable environmental conditions. Using the TOPSIS (Technique for Order Preference by Similarity to Ideal Solution) method, E8 was identified as the optimal composite formulation based on a multi-criteria evaluation of mechanical performance, density, and durability. The structure was then optimized using a Genetic Algorithm (GA) to minimize weight while satisfying mechanical constraints. The final GA-optimized design achieved a weight reduction of approximately 64.3% compared to a steel floor panel of equivalent size and load-bearing capacity, significantly improving transport efficiency. To verify structural performance, a finite element analysis (FEA) was conducted using Abaqus. The FEA results revealed a peak stress of 43.9 MPa, with stress concentrations localized in the central region of the panel. The Tsai-Wu failure index remained below 1.0 for all plies, indicating that no layer experienced failure under the design load. Evaluation using the Maximum Stress Theory further supported these results. The minimum factor of safety (FOS) was calculated as 2.19 in the transverse direction of Ply 1, which was the most critically stressed layer. This value not only exceeds the commonly accepted threshold for structural applications but also matches the design constraint of 2.0 set during the GA optimization based on the Tsai-Wu criterion. The FEA also confirmed the predicted deformation behavior, with a maximum displacement of 1.459 mm observed at the panel center—fully within serviceable limits. These results demonstrate that the composite is

capable of sustaining operational loads while maintaining dimensional stability and mechanical integrity. In conclusion, the integration of material selection (via TOPSIS)**,** design optimization (via GA), and structural validation (via FEA) has resulted in a high-performance, lightweight, and environmentally friendly composite panel. The use of locally available natural fibers and industrial byproducts not only reduces environmental impact but also supports regional resource utilization and circular economy goals. This study provides a viable path forward for the implementation of sustainable composite materials in transportation infrastructure and other structural engineering applications.

6.2 Future Research Directions

The primary goals for future research involve thoroughly evaluating the material's long-term performance and safety, enhancing its sustainability and manufacturing processes, analyzing its overall economic and environmental impact, and validating its performance in real-world applications.

Key areas for investigation include:

- Durability & Performance: Testing fatigue under cyclic loading and resistance to environmental aging (UV, temperature).
- Impact Assessment: Conducting life-cycle and cost-benefit analyses.
- Real-World Validation: Integrating the composite into full-scale structures (e.g., semi-trailers) to test its performance under service conditions.
- Fatigue testing is required as the component may be subjected to fatigue loads.

BIBLIOGRAPHY

[1] Asfaw KG. Investigation of the reasons for the unique growth and development of Agave species (Agave sisalana and Agave americana) crop plants at the southern, central, north western and eastern parts of tigray, Ethiopia. Curr Res J Biol Sci 2011;3:273–81.

[2] Melkamu A, Kahsay MB, Tesfay AG. Mechanical and water-absorption properties of sisal fiber (Agave sisalana)-reinforced polyester composite. J Nat Fibers 2018.

[3] Maurya HO, Gupta M, Srivastava R, Singh H. Study on the mechanical properties of epoxy composite using short sisal fibre. Mater Today Proc 2015;2:1347–55.

[4] Gupta M, Srivastava R. Properties of sisal fibre reinforced epoxy composite 2016.

[5] Pickering KL, Efendy MA, Le TM. A review of recent developments in natural fibre composites and their mechanical performance. Compos Part Appl Sci Manuf 2016;83:98–112.

[6] Assarar M, Scida D, El Mahi A, Poilâne C, Ayad R. Influence of water ageing on mechanical properties and damage events of two reinforced composite materials: Flax–fibres and glass–fibres. Mater Des 2011;32:788–95.

[7] Athijayamani A, Thiruchitrambalam M, Natarajan U, Pazhanivel B. Effect of moisture absorption on the mechanical properties of randomly oriented natural fibers/polyester hybrid composite. Mater Sci Eng A 2009;517:344–53.

[8] Chaudhary V, Bajpai PK, Maheshwari S. Effect of moisture absorption on the mechanical performance of natural fiber reinforced woven hybrid bio-composites. J Nat Fibers 2018.

[9] Costa F, d'Almeida J. Effect of water absorption on the mechanical properties of sisal and jute fiber composites. Polym-Plast Technol Eng 1999;38:1081–94.

[10] Joseph P, Rabello MS, Mattoso L, Joseph K, Thomas S. Environmental effects on the degradation behaviour of sisal fibre reinforced polypropylene composites. Compos Sci Technol 2002;62:1357–72.

[11] Fiore V, Di Bella G, Valenza A. The effect of alkaline treatment on mechanical properties of kenaf fibers and their epoxy composites. Compos Part B Eng 2015;68:14–21.

[12] Krishna KV, Kanny K. The effect of treatment on kenaf fiber using green approach and their reinforced epoxy composites. Compos Part B Eng 2016;104:111–7.

[13] Mohan T, Kanny K. Chemical treatment of sisal fiber using alkali and clay method. Compos Part Appl Sci Manuf 2012;43:1989–98.

[14] Noorunnisa Khanam P, Abdul Khalil H, Ramachandra Reddy G, Venkata Naidu S. Tensile, flexural and chemical resistance properties of sisal fibre reinforced polymer composites: effect of fibre surface treatment. J Polym Environ 2011;19:115–9.

[15] Otto GP, Moisés MP, Carvalho G, Rinaldi AW, Garcia JC, Radovanovic E, et al. Mechanical properties of a polyurethane hybrid composite with natural lignocellulosic fibers. Compos Part B Eng 2017;110:459–65.

[16] Premnath AA. Impact of surface treatment on the mechanical properties of sisal and jute reinforced with epoxy resin natural fiber hybrid composites. J Nat Fibers 2018.

[17] Rong MZ, Zhang MQ, Liu Y, Yang GC, Zeng HM. The effect of fiber treatment on the mechanical properties of unidirectional sisal-reinforced epoxy composites. Compos Sci Technol 2001;61:1437–47.

[18] Singha A, Rana RK. Natural fiber reinforced polystyrene composites: Effect of fiber loading, fiber dimensions and surface modification on mechanical properties. Mater Des 2012;41:289–97.

[19] Mbeche SM, Omara T. Effects of alkali treatment on the mechanical and thermal properties of sisal/cattail polyester commingled composites. PeerJ Mater Sci 2020;2:e5.
[20] Fiore V, Scalici T, Nicoletti F, Vitale G, Prestipino M, Valenza A. A new eco-friendly chemical treatment of natural fibres: Effect of sodium bicarbonate on properties of sisal fibre and its epoxy composites. Compos Part B Eng 2016;85:150–60.
[21] Bakri B, Putra A, Mochtar A, Renreng I, Arsyad H. Sodium bicarbonate treatment on mechanical and morphological properties of coir fibres. Int J Automot Mech Eng 2018;15:5562–72.
[22] Belaadi A, Amroune S, Bourchak M. Effect of eco-friendly chemical sodium bicarbonate treatment on the mechanical properties of flax fibres: Weibull statistics. Int J Adv Manuf Technol 2020;106:1753–74.
[23] Dos Santos JC, Siqueira RL, Vieira LMG, Freire RTS, Mano V, Panzera TH. Effects of sodium carbonate on the performance of epoxy and polyester coir-reinforced composites. Polym Test 2018;67:533–44.
[24] dos Santos JC, de Oliveira LÁ, Vieira LMG, Mano V, Freire RT, Panzera TH. Eco-friendly sodium bicarbonate treatment and its effect on epoxy and polyester coir fibre composites. Constr Build Mater 2019;211:427–36.
[25] Fiore V, Sanfilippo C, Calabrese L. Influence of sodium bicarbonate treatment on the aging resistance of natural fiber reinforced polymer composites under marine environment. Polym Test 2019;80:106100.
[26] Fiore V, Calabrese L. Effect of stacking sequence and sodium bicarbonate treatment on quasi-static and dynamic mechanical properties of flax/jute epoxy-based composites. Materials 2019;12:1363.
[27] Khalili P, Tshai KY. Comparative thermal and physical investigation of chemically treated and untreated oil palm EFB fiber. Mater Today Proc 2018;5:3185–92.
[28] Leman Z, Zainudin ES, Ishak MR. Effectiveness of alkali and sodium bicarbonate treatments on sugar palm fiber: mechanical, thermal, and chemical investigations. J Nat Fibers 2018.
[29] Zhou F, Cheng G, Jiang B. Effect of silane treatment on microstructure of sisal fibers. Appl Surf Sci 2014;292:806–12.
[30] Jeencham R, Suppakarn N, Jarukumjorn K. Effect of flame retardants on flame retardant, mechanical, and thermal properties of sisal fiber/polypropylene composites. Compos Part B Eng 2014;56:249–53.
[31] Gupta M, Deep V. Effect of water absorption and stacking sequences on the properties of hybrid sisal/glass fibre reinforced polyester composite. Proc Inst Mech Eng Part J Mater Des Appl 2019;233:2045–56.
[32] Das SC, Ashek-E-Khoda S, Sayeed MA, Paul D, Dhar SA, Grammatikos SA. On the use of wood charcoal filler to improve the properties of natural fiber reinforced polymer composites. Mater Today Proc 2021;44:926–9.
[33] Xanthos M. Functional fillers for plastics. John Wiley & Sons; 2010.
[34] Dinesh S, Kumaran P, Mohanamurugan S, Vijay R, Singaravelu DL, Vinod A, et al. Influence of wood dust fillers on the mechanical, thermal, water absorption and biodegradation characteristics of jute fiber epoxy composites. J Polym Res 2020;27:1–13.
[35] Ganapathy T, Sathiskumar R, Sanjay M, Senthamaraikannan P, Saravanakumar S, Parameswaranpillai J, et al. Effect of graphene powder on banyan aerial root fibers reinforced epoxy composites. J Nat Fibers 2021;18:1029–36.

[36] Saiteja J, Jayakumar V, Bharathiraja G. Evaluation of mechanical properties of jute fiber/carbon nano tube filler reinforced hybrid polymer composite. Mater Today Proc 2020;22:756–8.
[37] Borba PM, Tedesco A, Lenz DM. Effect of reinforcement nanoparticles addition on mechanical properties of SBS/Curauá fiber composites. Mater Res 2014;17:412–9.
[38] Chaudhary V, Rajput AK, Bajpai PK. Effect of particulate filler on mechanical properties of polyester based composites. Mater Today Proc 2017;4:9893–7.
[39] Devnani G, Sinha S. Effect of nanofillers on the properties of natural fiber reinforced polymer composites. Mater Today Proc 2019;18:647–54.
[40] Mohan K, Rajmohan T. Effects of MWCNT on mechanical properties of glass-flax fiber reinforced nano composites. Mater Today Proc 2018;5:11628–35.
[41] Nayak S, Nayak RK, Panigrahi I. Effect of nano-fillers on low-velocity impact properties of synthetic and natural fibre reinforced polymer composites-a review. Adv Mater Process Technol 2022;8:2963–86.
[42] Reddy BM, Reddy RM, Reddy BCM, Reddy PV, Rao HR, Reddy YM. The effect of granite powder on mechanical, structural and water absorption characteristics of alkali treated cordia dichotoma fiber reinforced polyester composite. Polym Test 2020;91:106782.
[43] Sarker F, Karim N, Afroj S, Koncherry V, Novoselov KS, Potluri P. High-performance graphene-based natural fiber composites. ACS Appl Mater Interfaces 2018;10:34502–12.
[44] CARDOSO BF de AF, RAMOS FJHTV, da SILVEIRA PHPM, da Silva FIGUEIREDO AB-H, GOMES AV, da VEIGA-JUNIOR VF. Mechanical and ballistic characterization of high-density polyethylene composites reinforced with alumina and silicon carbide particles. J Met Mater Miner 2022;32:42–9.
[45] Gebremeskel SA, Asija N, Chouhan H, Bhatnagar N. Appraisal of strain rate sensitivity of polypropylene nanocomposites. Procedia Eng 2017;173:800–6.
[46] Dias RR, Zattera AJ, Pereira IM, Soares BG. Ballistic impact performance of composite laminates based on high-density polyethylene/montmorillonite nanocomposite and Aramide fiber. Polym Compos 2021;42:5586–97. https://doi.org/10.1002/pc.26249.
[47] Haro EE, Odeshi AG, Szpunar JA. The Effects of Micro- and Nano-Fillers' Additions on the Dynamic Impact Response of Hybrid Composite Armors Made of HDPE Reinforced with Kevlar Short Fibers. Polym-Plast Technol Eng 2018;57:609–24. https://doi.org/10.1080/03602559.2017.1332207.
[48] Dharani Kumar S, Nitin MS, Kumar SS, Muthukumaran N, Magarajan U. Mechanical and ballistic performance of individual and synergistic filler reinforced glass fiber epoxy composites. Polym Compos n.d.;n/a. https://doi.org/10.1002/pc.29449.
[49] Kurdi MH, Al Ghafri K, Al Hamad F, Hassan K, Kurdi J, Michaud M. Ecofriendly conversion of marble waste into value-added tiles for green building. Innov. Technol. Adv. Sustain., CRC Press; 2024, p. 594–604.
[50] Awad AH, El-Gamasy R, Abd El-Wahab AA, Abdellatif MH. Assessment of mechanical properties of HDPE composite with addition of marble and granite dust. Ain Shams Eng J 2020;11:1211–7. https://doi.org/10.1016/j.asej.2020.02.001.
[51] Rama SR, Rai SK. Utilization of Granite Powder as Filler in PC-Toughened Epoxy Resins: Studies on Physico-Mechanical Properties. Polym-Plast Technol Eng 2011;50:1118–22. https://doi.org/10.1080/03602559.2011.566298.

[52] Awad AH, Abdel-Ghany AW, Abd El-Wahab AA, El-Gamasy R, Abdellatif MH. The influence of adding marble and granite dust on the mechanical and physical properties of PP composites. J Therm Anal Calorim 2020;140:2615–23. https://doi.org/10.1007/s10973-019-09030-w.
[53] Pour AK, Shirkhani A, Zeng J-J, Zhuge Y, Farsangi EN. Experimental investigation of GFRP-RC beams with Polypropylene fibers and waste granite recycled aggregate. Structures, vol. 50, Elsevier; 2023, p. 1021–34.
[54] Baviskar A, Bhamre V, Sarode S. Design and Analysis of a Leaf Spring for automobile suspension system: a review. Int J Emerg Technol Adv Eng 2013;3:407–10.
[55] Gebremeskel SA. Design, simulation, and prototyping of single composite leaf spring for light weight vehicle. Glob J Res Eng Mech Mech Eng 2012;12:21–30.
[56] Jancirani J, Assarudeen H. A review on structural analysis and experimental investigation of fiber reinforced composite leaf spring. J Reinf Plast Compos 2015;34:95–100.
[57] Patil JJ, Patil S. Design and Analysis of Composite Leaf Spring using Finite Element Methods-A Review. Int J Adv Engg TechVol VIssue IIApril-June 2014;58:59.
[58] Shokrieh MM, Rezaei D. Analysis and optimization of a composite leaf spring. Compos Struct 2003;60:317–25.
[59] Ekbote T, Sadashivappa K. Optimal design and analysis of mono leaf composite spring by finite element analysis, IEEE; 2012, p. 41–6.
[60] Ismaeel LMA. Optimization and static stress analysis of hybrid fiber reinforced composite leaf spring. Adv Mater Sci Eng 2015;2015.
[61] Ma L, He J, Gu Y, Zhang Z, Yu Z, Zhou A, et al. Structure design of gfrp composite leaf spring: An experimental and finite element analysis. Polymers 2021;13:1193.
[62] Wang L, Zhu C, Lu X, Zhang Z, Liang S. Structural design and analysis of sliding composite mono leaf spring. SAE Int J Commer Veh 2023;16.
[63] Yahaya R, Sapuan S, Jawaid M, Leman Z, Zainudin ES bin. Effect of layering sequence and chemical treatment on the mechanical properties of woven kenaf–aramid hybrid laminated composites. Mater Des 2015;67:173–9.
[64] Jenish I, Sahayaraj AF, Suresh V, Mani Raj J, Appadurai M, Irudaya Raj EF, et al. Analysis of the hybrid of mudar/snake grass fiber-reinforced epoxy with nano-silica filler composite for structural application. Adv Mater Sci Eng 2022;2022:1–10.
[65] ASTM International. Standard test method for tensile properties of plastics. ASTM international; 2014.
[66] ISO I. 179-1: 2010 Plastics—Determination of Charpy impact properties—Part 1: Non-instrumented impact test. ISO Geneva Switz 2010.
[67] ASTM S. Standard test methods for flexural properties of unreinforced and reinforced plastics and electrical insulating materials. ASTM D790. Annu Book ASTM Stand 1997.
[68] ASTM International. Standard test method for water absorption of plastics. D570-98 (Reapproved 2010) 2010.
[69] ASTM Committee D-20 on Plastics. Section D20. 70.01. Standard test methods for density and specific gravity (relative density) of plastics by displacement, American Society for Testing and Materials; 1991.

APPENDICES

Appendix A1: Objective function

```
function v = loading floor(x)
L1=13.5;% length
b=2.502;% width
dens=1.45e3;%density of E8
t1=x(1);t2=x(2);t3=x(3);
v=(L*b*((t1+t2+t3)*dens);% mass of the loading floor
```

Appendix B2: GA Optimization

```
lb = [0  0  0];
ub = [10 10 10];
opts = optimoptions(@ga, ...
                    'PopulationSize', 150, ...
                    'MaxGenerations', 200, ...
                    'EliteCount', 3, ...
                    'FunctionTolerance', 1e-8, ...
                    'PlotFcn', @gaplotbestf);
X0 = [0 0 0]; % Start point (row vector)
options.InitialPopulationMatrix = X0;
[xbest  fbest] = ga(@loading floor, 3 , [] , [] , [],  [],  ...
   lb , ub,  @loading floor constraints);
display (xbest)
display (fbest)
```

Appendix A3: Constraints

The ply angle orientation in the composite laminates is varied by altering the value of θ within the constraint function during the optimization process. The laminate stacking sequences evaluated in this study include a range of symmetrical and asymmetrical configurations to assess their impact on mechanical performance. The specific orientations analyzed are [0°/90°/0°], [45°/45°/45°], [0°/0°/0°], [0°/45°/0°], [45°/–45°/45°], [90°/0°/90°], [90°/45°/90°], [90°/90°/90°], and [45°/0°/45°]. These configurations are selected to explore the effects of different ply alignments on strength, stiffness, and failure response under operational loading conditions.

Constraint Function

```
%constraint function
function [c,ceq]=myconstraint(x)
M=P*L; %The bending moments of the loading floor
R=2; % margin of safety
% Mechanical properties
 E1=7.21 e9;    %Longitudinal modules in pa
 E2=3.12e9;   % Transverse modulus in pa
 V12=0. 0.32;
 G12=2.5e9; %In plane shear modulus in pa
 Xt=107.9e6; %Longitudinal tensile strength in pa
 Xc=-76.19e6; %Longitudinal compression strength in pa
 Yt=57.34e6; %Transvers tensile strength in pa
 Yc=-32.12e6; %Transvers compression strength in pa
 xy=29.45e6; %Shear strength in pa
 theta=[0 90 0];
 N=3; %layer number
% reduced stiffness matrix calculation
V21=V12*E2/E1;
Q11=E1/(1-(V12*V21));
Q12=(V12*E2)/(1-(V12*V21));
Q22=E2/(1-(V12*V21));
```

```
Q66=G12;
 % initialising the bending stiffness matrix
  D11=0;
  D12=0;
  D22=0;
  D66=0;
for i=1:N % layer number identifier
    deg=(theta(i))*pi/180;
    m=cos(deg);
    n=sin(deg);

    %transformed stiffness matrix
    Qbar11=(Q11*m^4)+(2*(Q12+(2*Q66))*(m^2)*(n^2))+(Q22*n^4);
    Qbar12=((Q11+Q22-(4*Q66))*(m^2)*(n^2))+(Q12*((m^4)+(n^4)));
    Qbar22=(Q11*(n^4))+(2*(m^2)*(n^2)*(Q12+(2*Q66)))+(Q22*m^4);
    Qbar66=(Q11+Q22-(2*Q12))*(m^2)*(n^2)+(Q66*((m^2)-(n^2))^2);

    %bending stiffness matrix
    D11storage=Qbar11*(((-(x(1)*(N-2*i)/2))^3-(-(x(1)*(N-2*(i-1))/2))^3)/3);
    D12storage=Qbar12*(((-(x(1)*(N-2*i)/2))^3-(-(x(1)*(N-2*(i-1))/2))^3)/3);
    D22storage=Qbar22*(((-(x(1)*(N-2*i)/2))^3-(-(x(1)*(N-2*(i-1))/2))^3)/3);
    D66storage=Qbar66*(((-(x(1)*(N-2*i)/2))^3-(-(x(1)*(N-2*(i-1))/2))^3)/3);

    D11=D11+D11storage;
    D12=D12+D12storage;
    D22=D22+D22storage;
    D66=D66+D66storage;
end
    D=[D11 D12 0; D12 D22 0; 0 0 D66];
    %calculating the mid surface curvatures
    K=D\M;
k=theta(1,1); % ply indicators
```

```
deg=(k)*pi/180;
   m=cos(deg);
   n=sin(deg);
 %transformed stiffness matrix
   Qbar11=(Q11*m^4)+(2*(Q12+(2*Q66))*(m^2)*(n^2))+(Q22*n^4);
   Qbar12=((Q11+Q22-(4*Q66))*(m^2)*(n^2))+(Q12*((m^4)+(n^4)));
   Qbar22=(Q11*(n^4))+(2*(m^2)*(n^2)*(Q12+(2*Q66)))+(Q22*m^4);
   Qbar66=(Q11+Q22-(2*Q12))*(m^2)*(n^2)+(Q66*((m^2)-(n^2))^2);
Qk=[Qbar11 Qbar12 0; Qbar12 Qbar22 0; 0 0 Qbar66];
zvalues=[(3*x(1))/2, x(1)/2] ; %z for upper and lower surface of the ply
%strains in a laminate
for j=1:length(zvalues)
   z=zvalues(j);
epsilonk=z.*K;

%stress in a laminate
sk=Qk*epsilonk;

%local stress
T=[m^2 n^2 2*m*n; n^2 m^2 -2*m*n; -m*n m*n m^2-n^2];
stress=T*sk;

%The components of the failure theory are found using the five strength parameters
F11=(-1/(Xt*Xc));
F22=(-1/(Yt*Yc));
F12=-0.5*(F11*F22)^0.5;
F66=1.0/xy^2;
F1=(1/Xt)+(1/Xc);
F2=(1/Yt)+(1/Yc);
F6=0;

%TSAI-WU Failure criterion
```

```
TS=((F1*stress(1,1)*R)+(F2*stress(2,1)*R)+(F6*stress(3,1)*R)+(F11*(stress(1,1))^2*(R^2))+(
F22*(stress(2,1))^2*(R^2))+(F66*(stress(3,1))^2*(R^2))+(2*F12*(stress(1,1))*(stress(2,1))))<1;
end
max_stress=max(sk); %display maximum stress value
t=3*x(1);
% All nonlinear constraints
c = [-t+(3*x(1)); t-(3*x(1)); TS];
% No equality constraints
ceq = [];
```